Investigation of the function of the PTPMEG2 phosphatase in mammalian autophagy

Estelle Descamps

University College London

and

The Francis Crick Institute

MPhil Supervisor: Dr Sharon A. Tooze

A thesis submitted for the degree of

Master of Philosophy

University College London

September 2020

Declaration

I, Estelle Descamps, confirm that the work presented in this thesis is my own. Where information has been derived from other sources, I confirm that this has been indicated in the thesis.

Abstract

Autophagy is a catabolic process that enables cells to engulf cytosolic components into a double-membrane vesicle called “autophagosome” to send them for lysosomal degradation. Autophagy occurs at a basal level to maintain cellular homeostasis but is dramatically induced by various stresses such as amino acid starvation to allow cells to generate new building blocks.

The autophagic response is mediated by many different actors, most of them from the ATG proteins family. Among those, ATG9A is particularly interesting since it is the only transmembrane protein required for autophagy and its function remains unknown. ATG9A localises on vesicles and tubular structures that seem to make brief interactions with the forming autophagosomes without completely fusing with them. Therefore, ATG9A is thought to promote the delivery of proteins or lipids to fuel the growth of nascent autophagosomes. Proteomic analysis of immunoisolated ATG9A vesicles revealed the presence of PTPMEG2 on ATG9A-positive membranes, a tyrosine phosphatase with no previously described role in autophagy.

In order to understand why PTPMEG2 is found on ATG9A-positive structures, I first assessed the impact of PTPMEG2 on the autophagic flux. However, the analysis of LC3 lipidation and of LC3 spots formation did not reveal any defect in the absence of PTPMEG2. Afterwards, I investigated the relationship between PTPMEG2 and ATG9A. My results suggest that the two proteins interact and that the localization of ATG9A is altered in the absence of PTPMEG2. As this phenotype is also observed upon loss of ARFIP2, another protein found on ATG9A vesicles, I then decided to explore the relationship between PTPMEG2 and ARFIP2 and confirmed that they interact with each other. Finally, I propose here a hypothetical model that integrates my data. However, more experiments are needed to better understand the possible interplay between ATG9A, PTPMEG2 and ARFIP2 in the distribution of ATG9A vesicles during autophagy.

Impact Statement

In October 2016, the Nobel Assembly made the decision to award the Nobel Prize in Physiology or Medicine to Yoshinori Ohsumi for his important contribution in the understanding of autophagy. At that time, most people in the general public had never heard of autophagy before and the attribution of the Nobel Prize helped to shed light on this cellular pathway and on its importance in human health and disease.

Autophagy is indeed a crucial process to maintain cellular homeostasis and to help cells cope with various stressful conditions, such as amino acid deprivation. The function of the autophagic pathway is to send elements of the cytoplasm to lysosomes for degradation. Once these elements are digested, the basic "building blocks" generated can be reused by the cell, making autophagy the cellular equivalent of our recycling system. Furthermore, the autophagic response can act on specific targets depending on the context. Damaged organelles or toxic molecules that threaten the cell function or pathogens in the case of an intracellular infection can all be selectively sent to lysosomes. Autophagy is therefore an invaluable response that allows cells to survive and thrive. Its dysregulation is known to be implicated in a number of diseases, such as Alzheimer's or Parkinson's where toxic protein aggregates accumulate in the cytoplasm of brain cells due to a defect in the autophagic pathway. Therefore, a better understanding of autophagy is absolutely crucial if we want to succeed in our fight against such terrible pathologies.

The autophagic response is mediated by a complex network of proteins and lipids. One of the most enigmatic protein of this machinery is ATG9A. The importance of ATG9A has been demonstrated by the major defects observed in autophagy upon its loss. However, its function still remains unclear. Consequently, the investigation of its role and regulation is now one of the hottest topics in the autophagy field. In this thesis, I focus on one of the proteins found enriched on ATG9A-positive structures, PTPMEG2. Not much is known

about this protein tyrosine phosphatase and it has never been studied in the context of autophagy before. Although the exploration of the link between PTPMEG2 and ATG9A presented here did not lead to any definitive answer or conclusion, the data I collected will hopefully serve as a good starting point for other projects carried out in our laboratory and will ultimately help improve our knowledge of the regulation of autophagy in different conditions.

Acknowledgement

First, I would like to thank my supervisor Sharon Tooze for welcoming me in her lab and at the Crick. I feel really lucky that I had the opportunity to study and to end my path in research in such an incredible environment. Thank you also for giving me the chance to take part in public engagement activities and to explore other career options, that was important for me and proved to be useful.

Many thanks to my thesis committee members Tim Levine, Michael Way and Sila Ultanir for their input, their useful comments and their continued support. Some students dread meeting their TC but I did not, as our meetings were always encouraging and helpful. Special thank you to Michael Way for being so supportive of my future career in teaching!

Thank you also to the invaluable Science Technology Platforms at the Crick and particularly to Mike Howell and his team for the high-throughput analysis of LC3 spots and to Nicola O'Reilly and her staff for the peptide arrays and immunogenic peptides production. Surely Crick scientists would feel lost without you.

Thank you to Sally Leevers and Caroline Ransom for your support and for making the PhD/MPhil journey of Crick students as smooth as possible.

Thank you to the past and present members of the MCBA lab for your help during these two years. Particular thanks go to Stefano, Javier and Wenxin for being such amazing friends in addition to being great labmates. You know how talkative I usually am but I cannot find words to describe how very grateful I feel to have met you. My life in the past two years would have been completely different without you and I will miss you so very much! Thanks also to Anais, Manue and Michael – you are all away now but certainly not forgotten. Finally, thank you to Harold for being so patient and helpful, even with a hundred things to do.

Massive thank you to Andy Harrison for being a top person and mentor. I did not have the chance to do as many activities with the Education team as I wanted (thanks Covid-19!) but I truly enjoyed the ones I did and that is mostly thanks to you. I am so grateful for the advice and support you provided me at a period when I really needed them. I hope I will be as good a teacher as you were and I will definitely try to come back and say hi with my future pupils!

A big thank you to all my friends from the Crick who made my days here so much better, and particularly to Stefano, Javier, Wenxin, Steinar, Felipe, Elina, Julia and Anqi. Thank you for the countless coffees, drinks, dinners and nights out. Thank you for putting up with me, my crazy ideas, my talkativeness and my changing mood sometimes. And most importantly, thank you for being equally present and caring through my highs and my lows. You were always there to lift me up when I needed. I will carry you all in my heart wherever I go and I wish you all the very best in life!

And finally thank you so much Cyril for being the best brother someone could wish for. No matter what, you always have my back and you always find the words to remind me of who I am and who I want to be. We have been through a lot and nevertheless you have become an amazing young man. I am so proud of you. Merci pour tout!

Table of Contents

Table of figures

List of tables

Abbreviations

αSNAP	α-soluble NSF attachment protein
AKT1S1	AKTI1 substrate 1
AP	Adaptor protein
ARFIP	Arfaptin
ATG	Autophagy-related
BafA1	Bafilomycin A1
BAR	Bin-Amphiphysin-Rvs
BIF-1	Endophilin B1
Cas9	CRISPR associated protein 9
CI-MPR	Cation-independent mannose-6-phosphate receptor
CMA	Chaperone-mediated autophagy
CRALBP	Cellular retinaldehyde-binding protein
CRISPR	Clustered regularly interspaced short palindromic repeats
CTL	Control
DEPTOR	DEP domain-containing mTOR-interacting protein
DFCP1	Double FYVE domain-containing protein 1
DMEM	Dulbecco’s modified Eagle medium
EBSS	Earle’s balanced salt solution
EEA1	Early endosome antigen 1
EGFR	Epidermal growth factor receptor
ER	Endoplasmic reticulum
ERBB2	Erb-b2 receptor tyrosine kinase 2
ERGIC	Endoplasmic reticulum-Golgi intermediate compartment
F	Fed
FIP200	FAK family kinase-interacting protein of 200 kDa
FHF	FTS-Hook-FHIP
GABARAP	GABA receptor-associated protein
GFP	Green fluorescent protein
HA	Hemagglutinin
HEK293A	Human embryonic kidney 293A

HOPS	Homotypic fusion and protein sorting
Hsc70	Heat shock cognate 70-kDa protein
HTS	High-throughput screening
IP	Immunoprecipitation
KO	Knock-out
LAMP2	Lysosome-associated membrane protein 2
LE	Longer exposure
mLST8	mTOR-associated protein LST8 homologue
mTORC1	Mechanistic target of rapamycin complex 1
NSF	N-ethylmaleimide-sensitive factor
OE	Overexpression
PAM	Protospacer adjacent motif
PC	Phosphatidylcholine
PE	Phosphatidylethanolamine
PI	Phosphatidylinositol
PI3P	Phosphatidylinositol-3-phosphate
PI4P	Phosphatidylinositol-4-phosphate
$PI(4,5)P_2$	Phosphatidylinositol-4,5-biphosphate
$PI(3,4,5)P_3$	Phosphatidylinositol-3,4,5-triphosphate
PI3K	Phosphatidylinositol-3-kinase
PI4K	Phosphatidylinositol-4-kinase
PNS	Post-nuclear supernatant
PS	Phosphatidylserine
PTP	Protein tyrosine phosphatase
PTPMEG2	Protein tyrosine phosphatase MEG2
RAB	RAS-related protein
RAPTOR	Regulatory associated protein of mTOR
RFP	Red fluorescent protein
RHEB	RAS homologue enriched in brain
RUSC2	RUN and SH3 domain containing 2
S	Starved
SB	Starved + bafilomycin A1 treated

SE	Short exposure
SEM	Standard error of the mean
Ser	Serine
SNARE	Soluble NSF attachment protein receptor
SNX18	Sorting nexin 18
SOD1	Superoxide dismutase 1
STAT3	Signal transducer and activator of transcription 3
STX	Syntaxin
TfR	Transferrin receptor
TGN	*Trans*-Golgi network
TRAPPIII	Transport protein particle III
TSC	Tuberous sclerosis complex
Tyr	Tyrosine
ULK	Unc51-like autophagy activating kinase
UVRAG	UV radiation resistance-associated gene protein
VAMP3	Vesicle-associated membrane protein 3
VEGFR2	Vascular endothelial growth factor receptor 2
VPS	Vacuolar protein sorting
WIPI2	WD40 repeat protein interacting with phosphoinositides 2

Chapter 1. Introduction

1.1. Autophagy: an overview

1.1.1. The different types of autophagy

Autophagy, from the Greek “self-eating”, primarily designates any pathway that sends cytosolic material to lysosomes for degradation. As such, three types of autophagy have been described: macroautophagy, microautophagy and chaperone-mediated autophagy (CMA) **(Figure 1.1)**. The latter two directly take place at the lysosome: microautophagy is characterized by the invagination of the lysosomal membrane to capture and digest small elements from the cytosol [1], while in CMA the protein chaperone Hsc70 (heat shock cognate 70-kDa protein) recognizes a specific motif in some proteins and translocates them into the lysosomal lumen through interaction with the lysosomal membrane protein LAMP2 (lysosome-associated membrane protein 2) [2]. Macroautophagy, on the other hand, differs from the two others in that it requires the formation of an intermediate and specific organelle, the “autophagosome”, to deliver cytosolic elements to the lysosome.

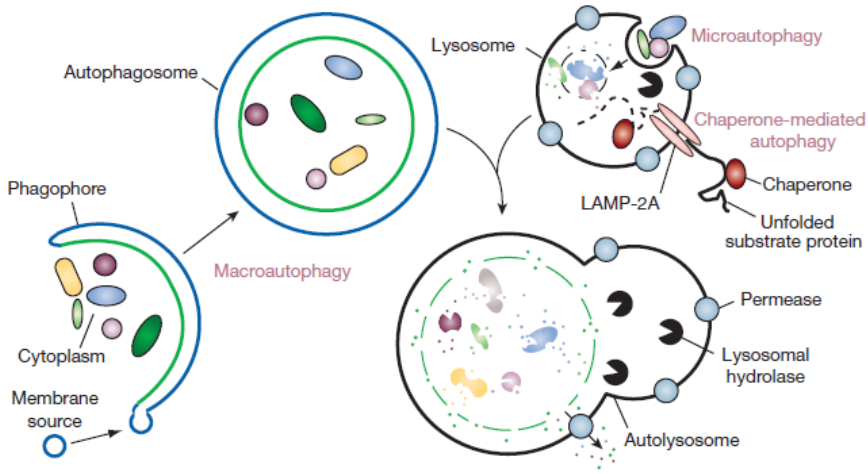

Figure 1.1: The three types of autophagy. The function of autophagy is to send cytosolic material to lysosomes for degradation. In macroautophagy, this is achieved by enclosing a portion of the cytosol in a vesicle called autophagosome that will later fuse with a lysosome. In microautophagy, the lysosomal membrane directly invaginates to capture elements of the cytosol. In chaperone-mediated autophagy, chaperones help to unfold and translocate cytosolic proteins into the lysosome. Illustration from [3].

Macroautophagy (hereafter simply named “autophagy”) is a highly conserved pathway, which is mediated and regulated by a complex network of proteins and lipids. The initiation of autophagy starts with the formation of a cup-shaped double-membrane structure (called “phagophore” or “isolation membrane”) that emerges from the endoplasmic reticulum and progressively encloses cytosolic material as it elongates. The phagophore eventually closes on itself to form a double-membrane vesicle called “autophagosome”. This autophagosome will later fuse with a lysosome, leading to the digestion of its content **(Figure 1.2)**. This degradation process hence generates new building blocks (such as amino acids, fatty acids, etc) that the cell can reuse, making autophagy a useful recycling system at the cellular level [4].

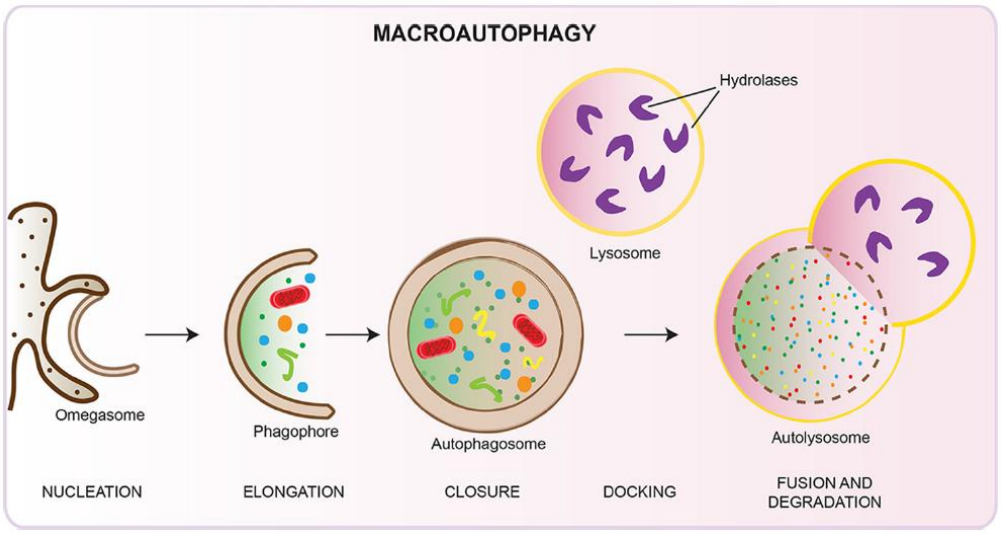

Figure 1.2: The macroautophagy process. Macroautophagy is characterized by the formation of a specific organelle (the autophagosome) to deliver cytosolic components to the lysosome for degradation. First, a double-membrane phagophore emerges from specific regions of the endoplasmic reticulum membrane called omegasomes. Then, the phagophore closes to create a double-membrane vesicle, named autophagosome, that contains a portion of the cytosol. Finally, the autophagosome fuses with a lysosome, which triggers the degradation and subsequent recycling of its content. Illustration from [5].

Autophagy occurs at a basal level in most tissues and cell types studied so far, although the extent and kinetics of the autophagic response vary greatly depending on the tissue [6]. It plays a crucial role in cellular homeostasis by ensuring the clearance of dysfunctional and damaged organelles and of toxic material such as protein aggregates. Moreover, autophagy can also be

significantly induced when needed, with a reported 10-fold or higher increase in the autophagic response when cells are exposed to stressful conditions [6]. Such stressors include nutrient starvation, growth factors depletion, low energy level, hypoxia, oxidative stress or microbial infection. Cells seem to induce autophagy in these conditions to either generate much needed building blocks or to eliminate the problematic element. Autophagy is therefore crucial for both cellular homeostasis and survival. Interestingly, it is worth noting that both basal and stress-induced autophagy use the same machinery and rely on the same regulatory mechanisms, indicating that cells are likely to constantly fine-tune the intensity of the autophagic process [6]. Finally, it has also been demonstrated that autophagy does not only degrade “bulk” portions of the cytosol but can also target specific structures to the lysosome. Indeed, several types of selective autophagy have been identified: mitophagy (for mitochondria), pexophagy (for peroxisomes), lipophagy (for lipid droplets), xenophagy (for microbes), etc [7]. The autophagic pathway is therefore a crucial and versatile response that ensures cell homeostasis and survival in a variety of situations.

In this thesis, I will focus on the most characterized subtype of autophagy: bulk macroautophagy induced by amino acid starvation.

1.1.2. Autophagy in health and disease

In addition to its role at the cellular level, autophagy is critical for a number of processes at the organismal level, throughout the lifetime of each individual. Indeed, autophagy is known to be induced as early as during development, partly due to the high demand for cellular “building blocks” during that period [8]. It is also crucially induced immediately after birth as the neonate stops feeding through the placenta. This requirement of autophagy for survival past the neonatal period has clearly been demonstrated in mice by the rapid death of newly born pups that lack key autophagy proteins [9]. Autophagy has also been reported to participate in the differentiation of some cell types, such as erythrocytes, and it is also involved in both innate and adaptative immunity [10,

11]. Finally, the progressive decline of autophagy with time has been linked to ageing, with some studies now focusing on the upregulation of autophagy to rejuvenate organisms and possibly extend lifespan [12-14].

Due to its potent and essential function in triggering the lysosomal degradation of cell components, autophagy needs to be tightly regulated. Therefore, it is not surprising that dysregulation of the autophagic pathway is linked to a wide range of diseases [11, 15]. In particular, a massive amount of research is focused on the link between autophagy defects and neurodegeneration [16]. Decrease or absence of autophagy in the brain leads to the accumulation of protein aggregates which can be very toxic if they are not eliminated. This often results in neuronal death and progressive loss of cognitive functions. In Alzheimer's disease, brain cells exhibit abnormal accumulation of the amyloid-β peptide and of the Tau protein. Studies now suggest that this accumulation can be caused by a decline in autophagy due to decreased levels of the protein Beclin1 [17] or by a defect in lysosomal activity which prevents the last step of autophagy and therefore affects the clearance of the toxic aggregates [18]. The crucial importance of autophagy has also been shown in Parkinson's disease, where neurons accumulate the protein α-synuclein which seems to inhibit autophagy, thus creating a vicious circle of further protein aggregation [19]. Autophagy is also increasingly studied in the context of cancer. The relationship between the two seems rather complex as autophagy has been reported to play both a tumour-suppressing and tumour-promoting role [20, 21]. Indeed, its function in eliminating potentially oncogenic stimuli such as leaky mitochondria makes autophagy a powerful mechanism to avoid cancer development. However, once a tumour is formed, it seems that autophagy could promote its growth by generating the nutrients cancer cells need to thrive. Overall, the role of autophagy in cancer is still poorly understood and probably depends on the type of cancer considered and its stage of development. To conclude, regardless of the disease considered, a better understanding of the autophagic pathway is absolutely essential in our fight to provide new and improved treatments to patients.

1.2. Molecular machinery of mammalian autophagy

While the first mention of the “autophagic vesicles” by Christian de Duve came from observations in mammalian cells, the big breakthrough in the field came from studies in the budding yeast *Saccharomyces cerevisiae*, years later, when the first genes involved in the regulation of autophagy were discovered. From 1992, Yoshinori Ohsumi published a series of groundbreaking results. Using a yeast line that accumulates autophagic vesicles due to a lack of vacuolar degradation enzymes [22], his team gradually identified several genes necessary for the autophagic response to nitrogen deprivation and named them *Apg*. The nomenclature was later unified and these genes are now called *Atg*, for “autophagy-related genes” [23]. Identification of *Atg* genes homologues in higher eukaryotes and characterization of the encoded ATG proteins quickly followed, with many of these proteins still being studied now.

The ATG proteins are commonly referred to as “the core machinery of autophagy”, due to their crucial function and requirement for the formation of autophagosomes. In mammals, the core machinery consists of the ULK protein kinase complex, the VPS34 lipid kinase complex, the PI3P effector WIPI2, and the ATG8 lipidation machinery **(Figure 1.3)**. I will describe the role of each of these key actors in this section, from the induction of autophagy to the formation of a mature autophagosome and the degradation of its content.

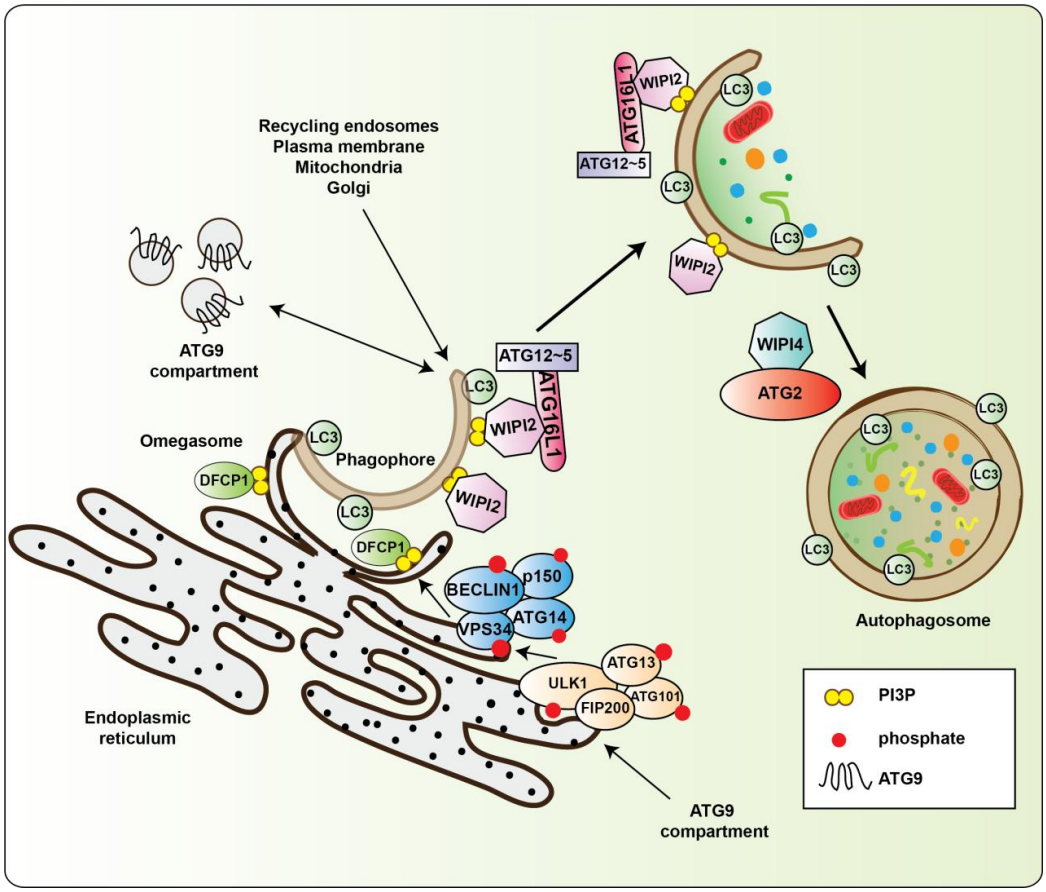

Figure 1.3: Overview of the autophagosome formation process in mammals. Upon autophagy induction, the ULK protein kinase complex activates the VPS34 lipid kinase complex I. VPS34 then starts producing PI3P which accumulates in a subregion of the endoplasmic reticulum – the omegasome – from where the phagophore originates. PI3P then recruits effectors that drive the lipidation of LC3 at the phagophore membrane. Vesicles from the ATG9A compartment are thought to promote both autophagy initiation and membrane expansion. The phagophore eventually closes on itself to form an autophagosome. Adapted from [5].

As previously mentioned, autophagy occurs at a basal level in most tissues but is dramatically induced when cells face stressful conditions such as nutrient deprivation, hypoxia or pathogen infection. Interestingly, most of the internal and external stimuli that influence autophagy are sensed and integrated by the same complex, mTORC1 (mechanistic target of rapamycin complex 1). mTORC1 acts as a major signaling hub for different pathways, turning on and off autophagy depending on the cell global situation [6]. This complex consists of the serine/threonine kinase mTOR and the non-catalytic subunits RAPTOR (regulatory associated protein of mTOR), DEPTOR (DEP domain-containing mTOR-interacting protein), AKT1S1 (AKTI1 substrate 1) and mLST8 (mTOR-

associated protein LST8 homologue). The activity of mTORC1 is positively regulated by RHEB (RAS homologue enriched in brain) and negatively regulated by the TSC1/2 (tuberous sclerosis complex 1/2) heterodimer, through RHEB inhibition [24]. In basal, unstressed conditions, mTORC1 is active and promotes anabolic processes like protein, lipid and nucleotide synthesis while suppressing catabolic activities such as autophagy [25]. However, in response to stress stimuli like amino acid starvation, mTORC1 is inactivated, thus releasing the brake on the autophagic pathway [24].

The most upstream complex in the hierarchy of the autophagic core machinery is the ULK complex. It is a protein kinase complex composed of the serine/threonine kinases ULK1/ 2 (unc51-like autophagy activating kinase 1/2) and the scaffolding proteins ATG13, ATG101 and FIP200 (FAK family kinase-interacting protein of 200 kDa). ULK1 and ULK2 seem to have redundant functions, with ULK1 being the most extensively described of the two. The main role of ATG101 is to stabilize the complex [26], while ATG13 and FIP200 help to promote the activation and translocation of the complex from the cytosol to the endoplasmic reticulum (ER), where it will induce autophagosome formation [27]. However, although the ULK complex is responsible for the initiation step of autophagy, it is worth noting that its formation does not depend on the nutrient status of the cell as the complex is found already formed and stable in the cytosol of fed cells [28].

In basal conditions, the activated mTORC1 binds ULK1 through its subunit RAPTOR and inhibits the ULK complex by phosphorylating ULK1 on Ser368 and Ser758 and ATG13 on Ser258, hence suppressing the autophagic response [5]. When mTORC1 gets inactivated in starved cells these inhibitory phosphorylations on ULK1 and ATG13 are removed. The activated ULK1 can then phosphorylate itself and its three binding partners to further activate the ULK complex and allow its translocation to the ER, where it will activate the VPS34 lipid kinase complex I [25].

There are two VPS34 complexes that are both crucial components of the autophagic pathway. The VPS34 core complex is composed of the subunits VPS34 (also called PI3KC3, class III phosphatidylinositol-3-kinase), p150 and Beclin1, to which associates either ATG14 or UVRAG (UV radiation resistance-associated gene protein), in a mutually exclusive way [29]. Association with ATG14 leads to the formation of the VPS34 complex I and to autophagosome nucleation, while binding to UVRAG forms the VPS34 complex II that acts later in the pathway.

Once the ULK complex is activated in starved cells, it phosphorylates VPS34, Beclin1 and ATG14 to enhance VPS34 lipid kinase activity [25]. The VPS34 complex I is then directed to the membrane of the ER by its ATG14 subunit [30]. There, VPS34 catalyses the transformation of phosphatidylinositol (PI) in phosphatidylinositol-3-phosphate (PI3P). This sudden production of PI3P on certain subregions of the ER is a key event in the formation of autophagosomes. These PI3P-enriched regions on the ER membrane are termed “omegasomes” and have been shown to act as a cradle for the nascent phagophore [31], making the VPS34 complex I the main actor of the autophagosome nucleation step.

The production of PI3P is essential for the phagophore to form and grow. First, thanks to its inverted cone shape, PI3P participates in the shaping of the phagophore by promoting a positive curvature bending of the membrane [32]. Second, the presence of PI3P attracts different effectors, namely DFCP1 (double FYVE domain-containing protein 1) and the WIPI proteins (WD-repeat domain phosphoinositide-interacting proteins). DFCP1 binds PI3P through its two FYVE domains and is one of the first PI3P effectors recruited [31]. It is therefore commonly used as a marker for omegasomes although its presence is not a requirement for autophagy and its function is unknown. There are 4 different WIPI (WD40 repeat protein interacting with phosphoinositides) proteins in mammals and each of them binds two molecules of PI3P. The most characterized is WIPI2, which is essential for autophagy because it links the

production of PI3P to the lipidation of ATG8 by binding ATG16L1 [33], as explained hereafter.

The lipidation machinery aims to covalently bind the soluble ATG8 proteins to the lipid phosphatidylethanolamine (PE) on both the inner and outer sides of the growing phagophore. This process is essential for the phagophore membrane to elongate and eventually close on itself to generate an autophagosome. Mammals count 6 members in the ATG8 protein family: LC3A, LC3B (the most common in starvation-induced autophagy), LC3C, GABARAP, GABARAPL1 and GABARAPL2. The structure of these proteins resembles ubiquitin and the lipidation machinery therefore comprises two “ubiquitin-like” conjugation systems [5, 25]. On one hand, ATG12 is conjugated to ATG5 by the E1-like ATG7 and the E2-like ATG10. The resulting ATG12-ATG5 conjugate then interacts with ATG16L1 to form the ATG12-ATG5-ATG16L1 complex that is recruited to the phagophore through the interaction of ATG16L1 with WIPI2 [33]. On the other hand, LC3s and GABARAPs are cleaved in the cytosol by ATG4 before being activated by the E1-like ATG7 and transferred to the E2-like ATG3. ATG8 proteins are finally covalently bound to PE by the ATG12-ATG5-ATG16L1 complex that acts like an E3-like enzyme. In this thesis, the cytosolic form of LC3B is abbreviated LC3-I, whereas the lipidated form that is conjugated to PE is referred to as LC3-II.

Finally, the elongated cup-shaped phagophore closes on itself to form an autophagosome, hence sequestering a portion of the cytosol. By then, most of the autophagy core machinery proteins have been removed from the autophagosomal membrane, with the notable exception of ATG8, which is thought to be involved in the closure mechanism. Lipidated LC3s and GABARAPs on the outer membrane of the autophagosome will eventually be cleaved off by ATG4 and recycled back to the cytosol, while ATG8 proteins bound to the inner membrane will be degraded upon fusion of the autophagosome with a lysosome [25]. This fusion event leads to the formation of an “autolysosome” and to the subsequent digestion of the engulfed cytosolic

material by lysosomal hydrolases. Although this final step is still not fully understood, several proteins have been reported to be involved in the fusion process, such as RAB7, STX17 and the HOPS complex [34, 35]. The VPS34 complex II also seems to play a crucial role, as UVRAG binds the HOPS complex subunit VPS16, which could help further activate RAB7 through VPS39, another subunit of the HOPS complex [32]. The recruitment of the phosphatidylinositol-4-kinase PI4KIIα on the autophagosomal membrane by GABARAP and the resulting PI4P production are also known to be required for the autophagosome-lysosome fusion step [36]. After fusion, both the autophagosome inner membrane and its sequestered content are degraded and the resulting “building blocks” generated are recycled back to the cytosol for the cell to reuse. The amino acids generated by this process are thought to re-activate mTORC1 at the surface of the lysosome and to act as one of the signals that terminate the autophagic response [6].

Despite the progress made in the last decades to better understand the formation of autophagosomes, many key questions remain unanswered. In particular, the mechanism by which the phagophore membrane grows is still poorly understood. It is believed that the phagophore expansion is probably fueled by some membrane input coming from multiple organelles, presumably the ER, the Golgi, the ER-Golgi intermediate compartment (ERGIC), the plasma membrane, mitochondria and recycling endosomes [37]. However, the exact source of this membrane supply and how it is transported to the site of autophagosome formation still need to be precisely determined. One of the current hypotheses in the field involves ATG9A-positive vesicles as possible carriers for the required lipids.

1.3. The special case of ATG9A

1.3.1. Mammalian ATG9A

Amongst the different ATG proteins, ATG9 is particularly interesting because it is the only transmembrane protein of the core machinery of autophagy. ATG9 homologues are found in all species from plants to humans and always seem to be required for autophagy. Two orthologues are found in mammals: the ubiquitously expressed ATG9L1 (hereafter called ATG9A) and ATG9L2, which is only found in the placenta and pituitary gland [38].

The requirement for ATG9A in mammalian autophagy has been demonstrated in multiple publications. Saitoh *et al.* generated a mouse model that is knock-out for ATG9A and showed that all the pups died within the first day following birth, indicating that ATG9A is necessary to survive the neonatal period when autophagy is known to be crucial [39]. At the cellular level, embryonic fibroblasts derived from this mouse line present a decreased number of LC3 spots formed upon starvation and a reduced degradation of long-lived proteins [39], as well as a defect in mitophagy [40]. The requirement of ATG9A for the formation of late autophagic structures (positive for LC3) but also of earlier structures (marked by ATG13, WIPI2 and ATG16L1) has consistently been demonstrated in other studies where ATG9A expression was depleted [41-43].

The crystal structure of human ATG9A has recently been characterized and revealed that ATG9A exists as a homotrimer with a complex internal network of cavities, including a central pore [44]. This hydrophilic pore connects both side of the membrane bilayer and is consistent with a putative role of ATG9A as a membrane transporter. Each of the three ATG9A protomers comprises four transmembrane helices with an additional two helices that are only partially embedded in the membrane, and the N-terminal and C-terminal tails of the protein are both cytosolic. While its transmembrane domains are highly conserved, the cytosolic tails of ATG9 differ in both length and sequence

between species [45]. The high-resolution structure also revealed that the C-terminal platform domain of ATG9A seems to be important for its interaction with other proteins [44].

1.3.2. Localization and trafficking

ATG9A presents an intriguing pattern of subcellular localization. In fed conditions, it is observed on both juxta-nuclear and peripheral structures. The juxta-nuclear pool seems to correspond to ATG9A on the *trans*-Golgi network (TGN), as it colocalizes with TGN46 and partially with GM130, whereas the peripheral pool appears to represent RAB11-positive recycling endosomes and late endosomes, where ATG9A colocalizes with RAB7 and RAB9 [43, 46]. Interestingly, in starved cells, ATG9A is significantly redistributed. Its presence on the juxta-nuclear pool decreases while it seems to further disperse in the cell periphery. This dispersal of ATG9A is reversed upon refeeding of the cells, indicating that ATG9A can cycle back to the TGN [43].

Surprisingly and unlike most other ATG proteins, ATG9A does not seem to be recruited on autophagic membranes. Despite its partial colocalization with ULK1, DFCP1, WIPI2, ATG16L1 and LC3, ATG9A appears to reside on vesicles that are distinct from phagophores and autophagosomes. Time-lapse microscopy experiments in starved cells revealed that ATG9A forms dynamic spots that briefly interact with both early and late autophagic structures, without any apparent fusion or stable incorporation [42, 47] **(Figure 1.4)**. Additional electron and X-ray microscopy experiments demonstrated that ATG9A is found on clusters of tubules and vesicles scattered in the cytosol and often found in close proximity to autophagosome formation sites and endosomes [42, 48]. This membranous structure has been named “the ATG9A compartment” **(Figure 1.5)** and seems to derive from the TGN and early, late and recycling endosomes, as subcellular fractionation showed a partial overlap of ATG9A with TGN46, EEA1 (early endosome antigen 1), CI-MPR (cation-independent mannose-6-phosphate receptor) and TfR (transferrin receptor) [42].

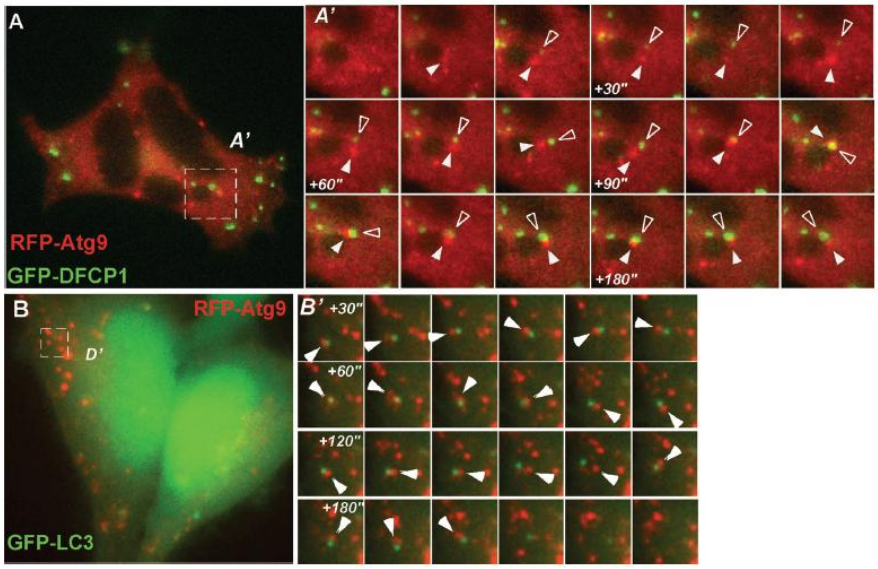

Figure 1.4: ATG9A vesicles transiently interact with phagophores and autophagosomes. Timelapse widefield microscopy of live, starved HEK293A cells co-expressing mRFP-ATG9A with either GFP-DFCP1 **(A)** or GFP-LC3 **(B)**. Magnified frames from the indicated regions are showed in A' and B'. Frames were acquired every 5 seconds, starting 5 minutes after the beginning of the starvation treatment. Every other frame is shown. Data from [42].

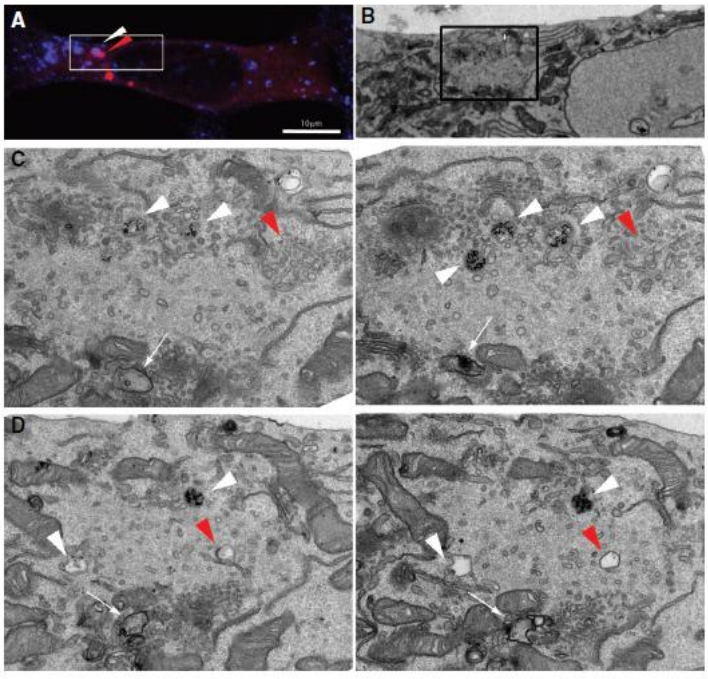

Figure 1.5: The ATG9A compartment. mRFP-ATG9A-positive structures and endosomes (positive for gold-labeled TfR) were identified in HEK293A cells by confocal light microscopy **(A)** before being imaged by electron microscopy **(B-D)**. Magnified frames of the boxed region in B are shown in C and D. ATG9A localizes on clusters of tubulo-vesicular structures (red arrowheads) found in the proximity of TfR-positive endosomes (white arrowheads) and nascent autophagosomes (white arrows). Data from [42].

The regulation of the trafficking of ATG9A is very complex and is still not fully understood. Several actors of the autophagy core machinery have been described to influence ATG9A localization. Indeed, depletion of ULK1 or ATG13 and inhibition of the PI3K complex all prevent ATG9A dispersal upon starvation [43, 49], whereas WIPI2 seems involved in the return of ATG9A vesicles to the Golgi complex after their interaction with omegasomes [42]. UVRAG has also been reported to promote ATG9A dispersal in starved cells by interacting with Beclin1 and the PI3K complex [50]. The interaction of UVRAG with BIF-1 (endophilin B1) is also crucial for the budding and fission of ATG9 vesicles from the Golgi [51] and the conjoint action of BIF-1, Dynamin-2 and SNX18 (sorting nexin 18) has also been demonstrated to mediate the formation of ATG9A vesicles from juxta-nuclear recycling endosomes [52, 53].

In addition to core autophagy proteins and their associated partners, AP complexes (adaptor protein complexes) also play a major part in the regulation of ATG9A trafficking. AP-4, in conjunction with its accessory protein RUSC2 (RUN and SH3 domain containing 2), is crucial for the formation of ATG9A vesicles from the Golgi [54, 55], while association of AP-4 with the FHF (FTS-Hook-FHIP) complex promotes the transport of ATG9A vesicles in the opposite direction, towards the centre of the cell [56]. Moreover, ATG9A has also been described to associate with the AP-1 and AP-2 complexes and this interaction is enhanced by the phosphorylation of ATG9A on Tyr8 by the Src kinase (in both fed and starved conditions) and on Ser14 by ULK1 (in starved conditions only). These phosphorylation events seem to have a synergistic effect on ATG9A dispersal and on basal and starvation-induced autophagy [57].

Finally, the TRAPPIII (transport protein particle III) complex has also been consistently described as a positive regulator of the retrograde transport of ATG9A from endosomes back to the Golgi apparatus, a step that seems important to sustain the autophagic response [46, 58, 59].

1.3.3. Proposed function

Despite its clear requirement in starvation-induced autophagy, the exact function of ATG9A remains to be established. As described before, ATG9A has been reported to briefly interact with both early and late autophagic structures, i.e. omegasomes, phagophores and autophagosomes [42] and to localize on key organelles for membrane traffic, such as the Golgi complex and recycling endosomes [42, 43]. Therefore, the current hypothesis of our team is that ATG9A vesicles could deliver lipids and/or proteins from different compartments to the forming autophagosome to promote its growth and function at different stages of the pathway.

Though likely, this hypothetic role for ATG9A has yet to be demonstrated. However, a recent publication from our laboratory seems to have identified the first reported cargoes delivered to the phagophore by ATG9A vesicles [60]. In order to better understand the function of ATG9A, Judith *et al.* immunoisolated ATG9A-positive membranes from fed and starved cells and submitted them to quantitative proteomics analysis **(Figure 1.6)**. The results showed an enrichment of ATG9A vesicles with phosphatidylinositol-metabolizing enzymes (namely PI4KIIα and PI4KIIIβ) and with BAR-domain containing proteins (such as ARFIP2 and BIF-1) in starved cells. Using various biochemical and cell biology techniques, Judith *et al.* further showed that the depletion of ARFIP2 leads to an increased dispersal of ATG9A in both fed and starved conditions. This dispersed localization is also observed for PI4KIIIβ and PI4P. Several experiments further suggested that PI4KIIIβ and PI4P are present on ATG9A vesicles and therefore come along with ATG9A when the vesicles disperse and transiently interact with early autophagic structures during starvation. Moreover, ARFIP2 also seems required for the integration of PI4KIIIβ and PI4P on ATG9A-positive membranes, as its absence depletes the levels of PI4KIIIβ and PI4P in the ATG9A immunoisolated compartment.

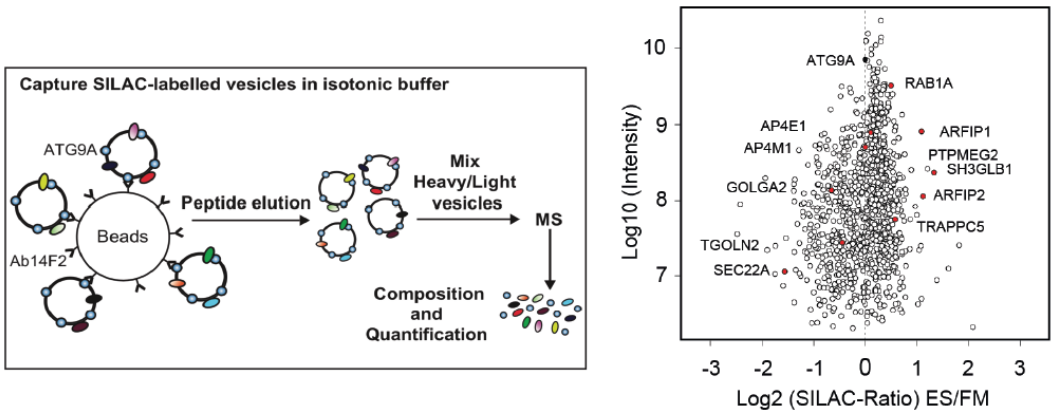

Figure 1.6: Immunoisolation and proteomics analysis of ATG9A-positive structures. ATG9A-positive membranes were isolated from fed and starved HEK293A cells using an antibody for endogenous ATG9A coupled to beads. The proteomic content of the isolated membranes was then analysed by mass spectrometry and shows an enrichment of BAR-domain containing proteins and a depletion of Golgi-associated proteins in starved conditions. Data from [60].

Based on this study, the current model therefore proposes that PI4KIIIβ and PI4P are present at the TGN with ATG9A in fed conditions but get loaded onto ATG9A vesicles upon starvation to be delivered at the autophagosome formation site and promote autophagy induction [60]. Furthermore, it seems that the delivery of PI4KIIIβ and PI4P leads to an early event in the pathway as it helps to direct ATG13 and the ULK complex to the autophagosome initiation site. This last observation is consistent with the previously described recruitment of ATG13 and ULK1 on the endoplasmic reticulum independently on PI3P production [41] and with the observation that ATG9A is necessary for the formation of early autophagic structures [40-42].

The complete analysis of the composition of the immunoisolated ATG9A-positive membranes performed in this study generated a long list of proteins, either enriched in fed or starved conditions, or detected at a similar level in both populations. Intriguingly, one of the top hits detected in this experiment is PTPMEG2, a protein tyrosine phosphatase with no previously described connection to autophagy.

1.4. The PTPMEG2 tyrosine phosphatase

1.4.1. Discovery

PTPMEG2 (also called PTPN9 or simply MEG2) is a class I, cysteine-based, non-receptor protein tyrosine phosphatase [61]. It was first described in 1992 when its cDNA sequence was cloned from the human MEG-01 megakaryocyte and human umbilical vein endothelial cell cDNA libraries [62]. Expression of this sequence led to the production of a 68-kDa protein made of 593 amino acids, with no apparent transmembrane domain, suggesting PTPMEG2 was cytosolic. The protein seems to be widely expressed in both human [62] and mouse tissues [63], with a particular enrichment in the brain and in leukocytes, which explains why many studies conducted on PTPMEG2 are done in mast cells, T lymphocytes and neutrophils.

1.4.2. Structure

The structure of PTPMEG2 is composed of two domains separated by a linker **(Figure 1.7)**. At the C-terminal end, PTPMEG2 contains a classical phosphatase domain (the PTP domain) that shares 30-40% identity with other known tyrosine phosphatases [62]. Unlike some dual-specificity phosphatases, the catalytic domain of PTPMEG2 only seems able to dephosphorylate tyrosine residues and has no effect towards serine or threonine residues, as tested on phosphorylated glycogen phosphorylase [62]. Remarkably, the PTP domain of PTPMEG2 is coupled to a putative lipid-binding domain (the Sec14 homology domain) at the N-terminal end of the protein. This domain is 24% homologous to the budding yeast protein SEC14p and 28% identical to the human cellular retinaldehyde-binding protein (CRALBP) [62], two proteins that have been described to bind lipids. CRALBP serves as a carrier protein for 11-*cis*-retinaldehyde and 11-*cis*-retinol in the human retina [64-66], whereas SEC14p mediates the exchange of phosphatidylinositol (PI) and phosphatidylcholine (PC) between membrane bilayers and is involved in protein transport through

the Golgi complex [67-69]. This association between a PTP catalytic domain and a Sec14 homology domain is unique amongst mammalian tyrosine phosphatases.

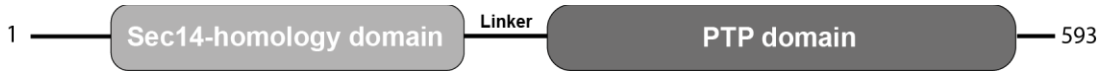

Figure 1.7: Schematic representation of PTPMEG2. The human PTPMEG2 protein is made of 593 amino acids and comprises two domains separated by a linker. The Sec14 homology domain is located at the N-terminal end of the protein, while the PTP domain is situated at the C-terminal end and is responsible for the tyrosine phosphatase activity of PTPMEG2.

1.4.3. Lipid binding

Given the particular structure exhibited by PTPMEG2, different studies were conducted to investigate the role of each domain and their possible interplay. Interestingly, the isolated PTP domain of PTPMEG2 has been demonstrated to be more active than the full-length protein, suggesting that the Sec14 domain could negatively regulate the catalytic activity of the PTP domain, at least until it binds lipids [70-72]. Several papers were indeed published on the interaction between the Sec14 homology domain of PTPMEG2 and different phospholipids, using either PIP strips (where phosphoinositides are bound to a membrane which is then incubated with the purified protein of interest), coated beads, or liposome assays. PTPMEG2 was mainly reported to bind to $PI(3,4,5)P_3$, $PI(4,5)P_2$ and PI4P with varying degrees of affinity [73, 74]. Furthermore, the interaction of the Sec14 domain with these lipids has been shown to enhance PTPMEG2 catalytic activity [71, 72]. One group also reported an interaction with phosphatidylserine (PS) [75] but this finding was not reproduced in other studies. Surprisingly, PTPMEG2 does not seem to bind to PI, one of the ligands of yeast SEC14p [73, 74]. A comparison of the putative structure of the Sec14 homology domain of PTPMEG2 with the crystal structure of yeast SEC14p reveals that the phospholipid-binding pocket of the Sec14 domain presents a

cluster of basic amino acid residues that are absent in SEC14p [74, 76]. This could explain why PTPMEG2 binds more acidic phosphoinositides than the unphosphorylated PI bound by SEC14p. Finally, despite the fact that it binds lipids, it is worth mentioning that no lipid transfer activity has been described for PTPMEG2 so far.

1.4.4. Localization

Despite the lack of transmembrane domain in the PTPMEG2 sequence, the protein is found both in the cytosol and associated to membranes. PTPMEG2 is indeed reported to localize on granules and phagosomes in neutrophils [72] and on secretory vesicles in mast cells and T cells [77]. Surprisingly, although PTPMEG2 is known to bind a subset of phosphoinositides, its lipid binding ability is only needed to support its catalytic activity and does not seem to be required for its membrane localization, suggesting that PTPMEG2 is targeted there by another mechanism [74]. Analysis of the localization of the two isolated domains shows that, while the PTP domain appears to be diffuse in the cytosol, the Sec14 domain displays a vesicular pattern of expression, suggesting that the Sec14 domain is responsible for PTPMEG2 targeting to membranes. A yeast two-hybrid screening followed by co-immunoprecipitation and immunofluorescence analysis revealed that ARFIP2 and a number of other vesicle-trafficking proteins interact with the Sec14 domain of PTPMEG2, providing a possible mechanism for the recruitment of PTPMEG2 to the cytosolic face of secretory vesicles [78].

1.4.5. Function

The combination of a putative lipid-binding domain with a tyrosine phosphatase domain raises many questions regarding the molecular role of PTPMEG2.

The most extensively described function for PTPMEG2 is the promotion of membrane fusion events between immature secretory vesicles. Indeed, the

overexpression of PTPMEG2 in rat mast cells and Jurkat T cells consistently induces a significant enlargement of secretory vesicles, on which PTPMEG2 localizes [74, 77]. Since these enlarged vesicles do not acquire markers for other organelles, they seem to originate from an enhanced homotypic fusion between immature secretory vesicles rather than from fusion with other structures [77]. Interestingly, this positive effect of PTPMEG2 overexpression on secretory vesicles fusion depends on both its catalytic activity [77] and its binding to $PI(3,4,5)P_3$ [74]. The molecular mechanism that underlies this process also involves the cytosolic protein N-ethylmaleimide-sensitive factor (NSF). NSF, with the help of αSNAP (α-soluble NSF attachment protein), is known to promote fusion events by disassembling *cis* complexes of SNARE (soluble NSF attachment protein receptors) proteins, allowing the SNAREs to participate in new rounds of fusion [79, 80]. However, this process is inhibited when NSF gets phosphorylated on Tyr83, in which case NSF binding to αSNAP is impaired. Dephosphorylation of NSF on this residue is performed by PTPMEG2, which therefore explains its positive effect on fusion when overexpressed [81]. Interestingly, the secretory vesicles on which PTPMEG2 resides in mast cells and Jurkat T cells are positive for $PI(3,4,5)P_3$. Therefore, upon binding of this lipid, the Sec14 domain of PTPMEG2 could activate the PTP domain, which would lead to NSF dephosphorylation, subsequent membrane fusion and ultimately, secretion [82] **(Figure 1.8)**.

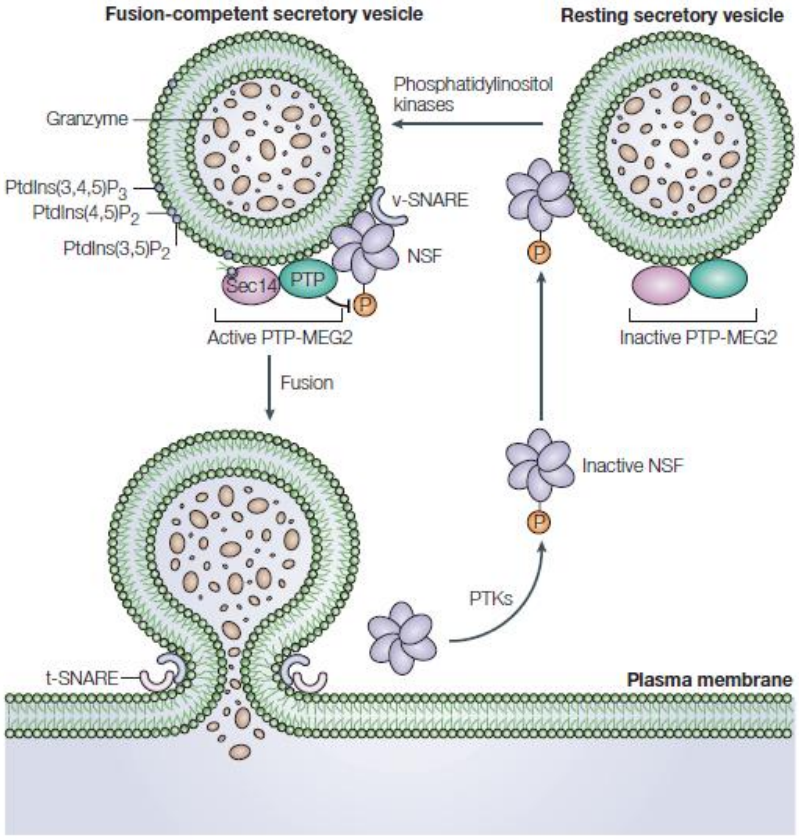

Figure 1.8: PTPMEG2 promotes membrane fusion events and secretion. PTPMEG2 is found associated to the membrane of secretory vesicles where its binding to a subset of phosphoinositides enhances its catalytic activity. PTPMEG2 can then dephosphorylate and activate NSF, which promotes membrane fusion events by disassembling SNARE *cis* complexes. Illustration from [82].

In an effort to further investigate the function of PTPMEG2, a PTPMEG2 knock-out (KO) mouse model was developed in 2005 [83]. The absence of PTPMEG2 leads to a very high rate of late embryonic lethality, with less than 10% of embryos surviving to birth and weaning. PTPMEG2 KO embryos display severe growth retardation, bone abnormalities, neural tube closure defects and hemorrhages **(Figure 1.9)**. At the cellular level, loss of PTPMEG2 impairs the activation of T lymphocytes and platelets, most likely due to observed defects in the secretion of interleukin-2 and platelet granules, respectively. This phenotype makes sense with the previously described role of PTPMEG2 in the fusion of immature secretory vesicles and secretion [81].

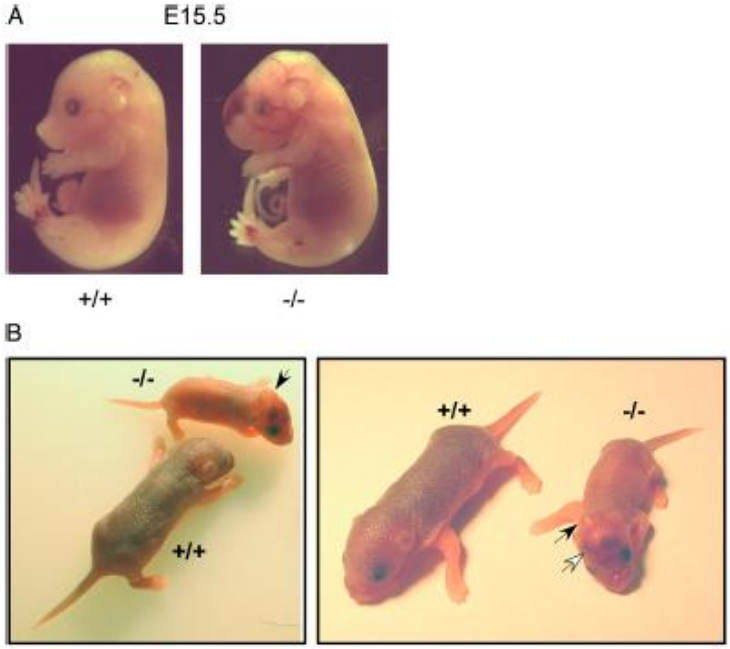

Figure 1.9: PTPMEG2 knock-out mice present severe developmental defects. A) PTPMEG2 KO embryos display craniofacial development defects and internal hemorrhages. They usually die before birth. **B)** The few PTPMEG2 KO pups that survive until the neonatal period are significantly smaller than their wild-type counterparts and present serious bone and craniofacial abnormalities (black arrows) and intracranial hemorrhages (white arrow). Pictures from [83].

In addition to its well described function in membrane fusion events, PTPMEG2 has also been reported to regulate different signaling pathways involved in a wide range of physiological and pathological processes. First, PTPMEG2 acts as a tumour suppressor in several different types of cancer (except in esophageal squamous cell carcinoma, where it seems to be an oncogene [84]). Indeed, it has been described to negatively regulate the development of breast cancer [85-88], hepatocellular cancer [89, 90], cervical cancer [91, 92], gastric cancer [93] and colorectal cancer [94]. In breast cancer, PTPMEG2 has been shown to exert its tumour suppressive function by dephosphorylating the EGFR (epidermal growth factor receptor) and ERBB2 (erb-b2 receptor tyrosine kinase 2) receptors and the downstream transcription activator STAT3 (signal transducer and activator of transcription 3) [87, 88]. PTPMEG2 has also been described as a negative regulator of insulin action and a promoter of gluconeogenesis, which makes it an interesting target to inhibit in the context of type-2 diabetes [95, 96]. Finally, PTPMEG2 is involved in the regulation of

erythropoiesis [97-99], vascular development and integrity (through VEGFR2 dephosphorylation) [100] and possibly brain development [101-103]. It is worth noting that the latter two could explain the phenotype of hemorrhages and brain malformation observed in the PTPMEG2 KO mouse model [83].

Interestingly, no link between autophagy and PTPMEG2 has been reported to date.

1.5. Hypothesis and aims

Despite the numerous studies demonstrating that ATG9A is required for starvation-induced autophagy, its exact function remains unknown. Young *et al.* first showed that mammalian ATG9A, which normally localizes on the Golgi complex and endosomes in fed conditions, disperses to the cell periphery upon amino acid starvation [43]. A few years later, Orsi *et al.* observed that the ATG9A-positive vesicles that disperse in starved cells seem to briefly interact with forming autophagosomes, without completely fusing with them [42]. With these findings in mind, ATG9A vesicles were quickly suggested to help promote autophagy by delivering lipids and/or proteins to the nascent autophagosome at different stages of its formation. This hypothetical function of ATG9A was later strengthened when Judith *et al.* analyzed the composition of ATG9A vesicles and found that these vesicles seemed to be responsible for the delivery of PI4P and PI4KIIIβ to the endoplasmic reticulum, where PI4P could then recruit ATG13 and thus initiate the autophagic response to starvation [60].

In their proteomic analysis of ATG9A-positive membranes, Judith *et al.* unexpectedly uncovered the presence of PTPMEG2, a protein tyrosine phosphatase with no previously described link with autophagy. PTPMEG2 is known to promote membrane fusion events [81] and could potentially transfer lipids, as its structure contains a Sec14 homology domain [62]. Interestingly, PTPMEG2 has also been reported to interact with ARFIP2 [78], another protein found on ATG9A vesicles [60]. Based on these observations, our hypothesis is

that PTPMEG2 could regulate autophagy by modulating ATG9A trafficking or function, either through its phosphatase activity, its role in membrane fusion, or its possible lipid transfer ability. Therefore, the aim of the present thesis is to investigate if PTPMEG2 has any impact on the autophagic response or on ATG9A trafficking, as well as to better understand and characterize the relationship between PTPMEG2, ARFIP2 and ATG9A.

Chapter 2. Materials & Methods

2.1. Cell culture and transfection

2.1.1. Cell culture and treatments

Dulbecco's Modified Eagle Medium-High Glucose (DMEM), trypsin-EDTA and fetal bovine serum (FBS) were purchased from Sigma. Earle's Balanced Salt Solution (EBSS) (5.56 mM D-glucose, 123.08 mM NaCl, 5.37 mM KCl, 1.82 mM $CaCl_2$, 0.81 mM $MgSO_4$, 0.99 mM Na_2HPO_4, 13.10 mM $NaHCO_3$) and Phosphate Buffered Saline (PBS) (137 mM NaCl, 3.4 mM KCl, 10 mM Na_2HPO_4, 1.8 mM KH_2PO_4, pH 7.2) were produced by the Cell Services facility team at the Francis Crick Institute. Cell culture vessels (flasks, dishes and plates) were obtained from Corning. To avoid detachment of HEK293A cells, all vessels except the flasks were treated for 10 minutes with 0.1 mg/mL poly-D-lysine (Sigma), then washed three times with distilled water and dried before seeding cells.

HEK293A cells were obtained from the Cell Services facility at the Francis Crick Institute. Control (CTL) and knock-out (KO) cell lines for PTPMEG2 were previously generated by Delphine Judith using the CRISPR-Cas9 technology [104].

Cells were rountinely maintained in DMEM supplemented with 10% FBS, 4.8 mM L-glutamine (Sigma) and 500U/mL penicillin + 100 µg/mL streptomycin (Pen-Strep) (Sigma) in humidified conditions at 37°C in 10% CO_2. In this thesis this medium is referred to as "full medium".

Once they reached about 90% confluency, cells were passaged by washing them once with PBS and incubating them in trypsin for 3 minutes. They were then typically split using a 1:10 dilution to maintain them in culture. Cells were discarded after they reached a passage number of about 20. To generate frozen vials, trypsinised cells from a confluent T75 flask were centrifuged at

1000 rcf for 5 minutes and resuspended in 1 mL of a 90% FBS-10% DMSO mixture. Aliquots of 1 mL were frozen and kept at -80°C before being handed to the Cell Services facility for long-term storage in liquid nitrogen. When needed, these vials were thawed and cells were reseeded in T75 flasks. The medium was changed the following day to remove the DMSO.

In “fed” conditions, cells were maintained in full medium, while in amino acid “starved” conditions (where autophagy is induced), cells were washed twice with EBSS and then incubated in EBSS for two hours at 37°C, 10% CO_2. Where indicated, cells were also treated for two hours with 100 nM bafilomycin A1 (Calbiochem) diluted in EBSS.

2.1.2. Transfection

When overexpressing tagged proteins, plasmid DNA transfection was performed in one day using Lipofectamine 2000 (Life Technologies) and OptiMEM (Life technologies).

First, cells were seeded so that the confluency would be around 80% prior to transfection on the next day. The following indications are for a 6-cm dish of HEK293A cells. Volumes of reagents were scaled up in other cases according to the surface ratio of the cell culture dish used. In one tube (Mix A), 500 µL OptiMEM was mixed with 4.8 µL Lipofectamine 2000, while in another tube (Mix B), 500 µL OptiMEM was mixed with 2 µg total DNA. The A and B mixtures were incubated separately for 5 minutes at room temperature then mixed together and incubated for a further 20 minutes. After removing full DMEM medium from the 6-cm dish and washing the cells once with OptiMEM, the A-B mixture was added. Cells were incubated with DNA for 4 hours at 37°C and 10% CO_2, before changing the medium back to DMEM. The transfected cells were ready to be seeded for experiments the next day.

2.2. Biochemistry

2.2.1. Antibodies

Table 2.1: Primary and secondary antibodies used for Western blots

PRIMARY ANTIBODIES					
Antigen	**Species**	**Antibody**	**Supplier**	**Dilution**	**Notes**
ARFIP2	Rabbit	40-2400	Invitrogen	1:500	
ATG9A	Rabbit	STO215	Homemade	1:1000	Young *et al.*, 2006 [43]
GFP	Mouse	3E1	CRUK	1:1000	
GFP	Rabbit	SC8334	Santa Cruz	1:1000	
HA.11	Mouse	MMS-101R	Covance	1:1000	
HA.11	Rabbit	PRB-101P	Covance	1:1000	
LC3B	Rabbit	ab48394	Abcam	1:1000	
PTPMEG2	Mouse	MAB2668	R&D Systems	1:500	
SOD1	Rabbit	ab16831	Abcam	1:2000	
STX6	Rabbit	110 062	Synaptic Systems	1:2000	
VAMP3	Rabbit	V31 & V32	Andrew Peden	1:500	
VINCULIN	Mouse	V9264	Sigma	1:5000	

SECONDARY ANTIBODIES			
Antigen	**Conjugated to**	**Supplier**	**Dilution**
Rabbit IgG	HRP	GE Healthcare	1:5000
Mouse IgG	HRP	GE Healthcare	1:5000

2.2.2. Cell lysis for Western blot

After being treated as indicated (starvation or else), cells were transferred on ice and washed twice with cold PBS. They were then incubated for 5 minutes in cold TNTE lysis buffer (20 mM Tris-HCl pH 7.5, 150 mM NaCl, 5 mM EDTA, 0.3% Triton X-100) supplemented with 1x EDTA-free complete protease inhibitor cocktail (Roche). The volume of lysis buffer used was typically 100 µL/well for each well of a 12-well plate with volumes scaled up in other cases according to the surface ratio of the cell culture dish used. Cells were then scraped and the lysate was collected in a clean tube. Following a 10-minute centrifugation at 13200 rcf at 4°C, the post-nuclear supernatant was collected in a new tube and mixed with 5x SDS sample buffer (15% SDS (w/v), 213.5 mM Tris-HCl pH 6.8, 50% glycerol (w/v), 16% β-mercaptoethanol, bromophenol blue) to a final concentration of 1x. Lysates were then heated at 65°C for 10 minutes, briefly mixed and spun down before analysis by SDS-PAGE.

2.2.3. SDS-PAGE and protein transfer

Samples were loaded on NuPAGE 4-12% Bis-Tris precast gels (Life Technologies) and electrophoresis was performed in either MES (1x: 50 mM MES, 50 mM Tris Base, 0.1% SDS, 1 mM EDTA, pH 7.3) (Novex) or MOPS (1x: 50 mM MOPS, 50 mM Tris Base, 0.1% SDS, 1 mM EDTA, pH 7.7) (Novex) running buffer at 200 V until the dye front reached the bottom of the gel (after about 50 minutes). At this stage, the gel was carefully collected and proteins were transferred to a 0.45 µm polyvinylidene fluoride (PVDF) membrane (Merck Milipore), which had previously been quickly soaked in methanol (Fisher Chemical). Wet transfer was achieved using the Genie Blotter system (Idea Scientific Company) and a so-called “sandwich” containing the gel, the membrane, thick paper sheets and transfer sponges, immerged in transfer buffer (20% methanol, 150 mM glycine, 20 mM Tris base). Proteins were transferred at 4°C for about 60-90 minutes at 27 V. In order to check the

efficiency of the transfer, membranes were then incubated in Ponceau S stain (Sigma) for 15 minutes, washed with distilled water and scanned. They were then briefly washed with PBS prior to blocking.

2.2.4. Western blotting and detection

Following Ponceau S destain, membranes were blocked for 30 minutes in 5% powdered skimmed milk (w/v) (Sigma) in 0.1% PBSA-Tween 20 (hereafter noted PBS-T). Once blocked, membranes were then incubated overnight at 4°C with primary antibody solutions, diluted in 5% milk in PBS-T as indicated in **Table 2.1**. The next morning, membranes were washed three times in PBS-T and incubated with HRP-conjugated secondary antibody solutions diluted in 5% milk in PBS-T as indicated in **Table 2.1**, for 1 hour at room temperature. After three more washes with PBS-T, membranes were placed on a flat, clean glass plate and incubated with either ECL (Amersham, GE Healthcare) or Luminata Classico/Crescendo Western HRP substrate (Merck Milipore) for 1-2 minutes. The chemiluminescence signal obtained was detected using the Imager 680 blot and gel developer (Amersham, GE Healthcare). Various exposure times were applied depending on the experiment.

When the membrane needed to be re-probed for a different protein, membranes were first incubated in stripping buffer (200 mM glycine, 1% SDS (w/v), pH 2.5) (Thermo Scientific) for 10 minutes. After being thoroughly washed 5 times with PBS-T, they were then blocked in 5% milk in PBS-T for 30 minutes and later incubated with primary and secondary antibody solutions as described above.

2.2.5. Crude subcellular fractionation

Cells were seeded in 15-cm dishes which were previously coated with poly-D-lysine. The seeding density was 9×10^6 cells per dish for the analysis of endogenous proteins and 2×10^6 cells per dish when looking at overexpressed

proteins. In this last case, transfection was performed the day after seeding and cells were lysed the day after transfection.

On the day of extraction, cells were washed once with PBS and then once briefly with HB buffer (20 mM HEPES-KOH pH 7.5, 2.5 mM MgOAc, 1 mM EDTA, 1 mM dithiothreitol (DTT) and 250 mM sucrose) supplemented with 1x EDTA-free complete protease inhibitor cocktail (Roche). The buffer used for the wash was quickly removed and cells were incubated for 10 minutes on ice with 1 mL of fresh HB buffer. Following incubation, cells were scraped and collected in a clean tube. Cells were then lysed on ice by passing them through a 25-gauge needle (BD Microlance) 10 times, using a 1-mL syringe (BD Microlance). Trypan Blue staining (Gibco) was used to check cell breakage.

At this stage, the lysates were centrifuged for 5 minutes at 3000 rpm and at 4°C. Post-nuclear supernatants were collected in new tubes with 100 µL saved for future Western blot analysis. The rest was centrifuged in an ultracentrifuge tube at 47000 rpm for 1 hour at 4°C in a benchtop ultracentrifuge. Following this, the supernatant (which corresponds to the cytosolic fraction) was transferred in a new tube while the pellet (which corresponds to the membrane fraction) was resuspended in HB buffer and sonicated for 1 minute (with intervals of 10 seconds sonication and 10 seconds recovery alternating).

All samples were mixed with 5x SDS sample buffer and processed for Western blot analysis as described above.

2.2.6. Immunoprecipitation

For immunoprecipitation experiments of endogenous PTPMEG2, 6 x 10^6 cells were seeded per condition in 15-cm dishes, which were previously coated with poly-D-lysine.

The next day, cells were washed twice with cold PBS then harvested and incubated on a wheel for 1 hour at 4°C in 800 µL of LMNG lysis buffer (20 mM Tris-HCl pH 7.5, 150 mM NaCl, 5 mM EDTA, 1% LMNG) supplemented with 1x EDTA-free complete protease inhibitor cocktail (Roche). Following a 15-minute centrifugation at 13200 rcf at 4°C, the post-nuclear supernatant was collected in

a new tube. At this stage, 25 µL of empty beads were added to preclear the lysates. The mixture was incubated on a wheel for 1 hour at 4°C. The supernatant (corresponding to the precleared lysate) was then transferred to a new tube and about 20 µL of it were collected at this stage for future Western blot analysis of the "input". The protein concentration was measured to normalize all samples.

The post-nuclear supernatant was then split in half and incubated overnight at 4°C on a wheel with beads conjugated to either the PTPMEG2 antibody or the purified mouse IgG antibody which was used as control. In both cases, 50 µL of Protein G Dynabeads (Invitrogen) were mixed to 5 µg of antibody (per dish).

The next day, about 40 µL of the supernatant was collected for future Western blot analysis of the "unbound" fraction, the rest was discarded. The remaining beads pellet was then washed 3 times with cold LMNG lysis buffer. After the last wash, all the supernatant was carefully discarded to minimise dilution of the beads. The pellet was then resuspended in 2x SDS sample buffer to a final of 1x and samples were analysed by Western blot as described above.

For immunoprecipitation experiments of overexpressed proteins using GFP-TRAP beads (ChromoTek), 2 x 10^6 cells were seeded per condition in 10-cm dishes, which were previously coated with poly-D-lysine. Cells were transfected the day after seeding and lysed the day after transfection.

On the day of protein extraction, cells were washed twice with cold PBS before being incubated for 10 minutes in 500 µL of cold NP40 lysis buffer (20 mM Tris-HCl pH 7.5, 150 mM NaCl, 5 mM EDTA, 1% NP40) supplemented with 1x EDTA-free complete protease inhibitor cocktail (Roche). Cells were then scraped and the lysate was collected in a clean tube. Following a 10-minute centrifugation at 13200 rcf at 4°C, the post-nuclear supernatant was collected in a new tube. At this stage, 10 µL of blocked agarose beads were added to preclear the lysates. The mixture was incubated on a wheel for 1 hour at 4°C, then centrifuged for 5 minutes at 13200 rcf at 4°C. The supernatant (corresponding to the precleared lysate) was transferred to a new tube and

about 40 µL of it were collected at this stage for future Western blot analysis of the “input”.

The post-nuclear supernatant was then incubated for 2 hours at 4°C on a wheel with 15 µL of a 50% slurry of GFP-TRAP beads (i.e. with 7.5 µL of beads). These beads were previously washed using cold lysis buffer.

After the incubation, the lysate-beads mixture was centrifuged for 5 minutes at 13200 rcf at 4°C. About 40 µL of the supernatant were collected for future Western blot analysis of the “unbound” fraction, the rest was discarded. The remaining beads pellet was then washed 3 times with cold NP40 lysis buffer, centrifuging and removing the supernatant at each step. After the last wash, all the supernatant was carefully discarded to minimise dilution of the beads. The pellet was then resuspended in 2x SDS sample buffer to a final of 1x and samples were analysed by Western blot as described above.

2.3. Imaging

2.3.1. Antibodies

Table 2.2: Primary and secondary antibodies used for immunofluorescence experiments

PRIMARY ANTIBODIES					
Antigen	**Species**	**Antibody**	**Supplier**	**Dilution**	**Notes**
ARFIP2	Rabbit	40-2400	Invitrogen	1:300	
ATG9A	Hamster	14F2	Homemade	1:500	Judith *et al.*, 2019 [60]
GM130	Mouse	610822	BD Biosciences	1:500	
LC3B	Rabbit	ab48394	Abcam	1:2500	Methanol permeabilisation

SECONDARY ANTIBODIES			
Antigen	**Conjugated to**	**Supplier**	**Dilution**
Rabbit IgG	Alexa Fluor 488	Life Technologies	1:1000
Mouse IgG	Alexa Fluor 647	Life Technologies	1:1000
Hamster IgG	Cy3	Jackson ImmunoResearch	1:500

2.3.2. Immunofluorescence labelling

For immunofluorescence experiments imaged by confocal microscopy, 8 x 10^4 cells were seeded onto coverslips which were previously coated with poly-D-lysine. The next day, cells were treated under indicated conditions (starvation or else) before being fixed for 20 minutes in 3% paraformaldehyde (Agar Scientific) in PBS supplemented with 0.01 mM $CaCl_2$ and 0.01 mM $MgCl_2$. Cells were then washed three times in PBS and treated with 50 mM NH_4Cl (BDH Laboratory Supplies) for 10 minutes to quench any unbound paraformaldehyde groups and hence reduce autofluorescence. After three more washes in PBS, cells were permeabilised in PBS containing 50 µg/mL digitonin (Merck Milipore)

for 2 minutes or in methanol (Fisher Chemical) for 5 minutes (in the case of LC3 staining only) and washed again three times in PBS. Cells were then blocked in 5% BSA fraction V (Roche) in PBS for 30 minutes. Afterwards, coverslips were placed in a humidified chamber and incubated for 1 hour with primary antibodies diluted in PBS with 1% BSA as indicated in **Table 2.2**. They were then washed three times in PBS, placed back in the humidified chamber and incubated in the dark for 1 hour with secondary antibodies diluted in PBS with 1% BSA as indicated in **Table 2.2**. After three more washes, cells were treated with 5 µg/mL Hoechst (Sigma) in PBS for a few seconds to stain nuclei, then washed twice with PBS and once with water. Finally, coverslips were mounted onto microscope slides using Mowiol 4-88 (Calbiochem) and stored in the dark at 4°C. All these steps were carried out at room temperature unless stated otherwise.

For immunofluorescence experiments analysed by high-throughput screening, 2.5×10^4 cells were seeded per well in a 24-well microplate with a flat and clear bottom (Ibidi) which was previously coated with poly-D-lysine. The protocol followed was essentially the same as described above except that the primary and secondary antibody solutions were directly added to the wells (150 µL/well). After all the stainings were done, cells were left in PBS and the plate was sealed and kept at 4°C in the dark until its reading.

2.3.3. Confocal microscopy

Cells on coverslips were imaged using a Zeiss Axioplan 2 LSM880 laser-scanning confocal microscope with a 63x, 1.4 NA oil-immersion objective (Carl Zeiss MicroImaging, Inc). The slice thickness was 0.8 µm. Laser settings were kept constant between images and conditions within the same experiment to allow comparison.

2.3.4. High-throughput screening

For high-throughput, automated counting of LC3 spots, cells in 24-well, clear-bottom microplates were imaged and analysed using the Opera Phenix High-Content Screening System and the associated Harmony software (PerkinElmer). Images were collected using the confocal mode with 40x magnification and 90 fields imaged per well.
Imaging of the plates and data collection were kindly carried out by the High-Throughput Screening (HTS) facility team at the Francis Crick Institute.

2.4. Molecular biology

2.4.1. Bacterial transformation

Aliquots of 25 µL of chemically competent *E. coli* bacteria (DH5α strain) (Life Technologies) were thawed on ice. Bacteria were then mixed to about 500 ng of plasmid DNA and incubated on ice for 30 minutes. Afterwards, bacteria were heat-shocked at 42°C for 30 seconds to allow DNA penetration and placed back on ice for a further 2 minutes. At this stage, 900 µL LB medium (1% bacto-tryptone (w/v), 0.5% yeast extract (w/v), 170 mM NaCl) (Media preparation facility, The Francis Crick Institute) were added in each tube and the bacteria were placed in an Eppendorf thermomixer set on 500 rpm at 37°C for 1 hour. About 100 µL of the transformed bacteria were then spread onto LB-agar plates (1% bacto-tryptone (w/v), 0.5% yeast extract (w/v), 170 mM NaCl, 1.5% agar) (Media preparation facility, The Francis Crick Institute) which contained either ampicillin (100 mg/mL) or kanamycin (50 mg/mL) as a selection marker. The plates were then incubated upside down overnight at 37°C for bacterial colonies to grow.

2.4.2. Plasmid DNA extraction

The next day, individual bacterial colonies were picked over a flame and used to inoculate 5 mL (for minipreps) or 250 mL (for maxipreps) starter cultures of LB medium containing the appropriate antibiotic. Bacterial cultures were then left to grow overnight in a shaking incubator at 37°C. The next morning, the cultures were pelleted at 4122 rcf for 15 minutes. For miniprep plasmid DNA purification, bacteria pellets were handed to and processed by the Genomics Equipment Park facility team at the Francis Crick Institute. For maxiprep plasmid DNA purification, the Nucleobond Xtra Midi Plus kit (Macherey-Nagel) was used as per manufacturer's instructions. The precipitated DNA obtained was dissolved in TRIS buffer. DNA concentration was then measured using a Nanodrop spectrophotometer (Thermo Scientific) and adjusted to reach a final concentration of 1 µg/µL.

2.4.3. Sequencing

Mini- and midipreps were sequenced using capillary sequencing on an Applied Biosystems 3730XI DNA analyser by the Genomics Equipment Park facility team at the Francis Crick Institute.

2.4.4. Plasmids

Table 2.3: Plasmids used in this thesis

Name	Insert	Vector	Resistance	Source
HA	Empty	pDEST-HA	Ampicillin	T. Johansen
HA-PTPMEG2	PTPMEG2	pDEST-HA	Ampicillin	D. Judith
HA-Sec14	Sec14 domain	pDEST-HA	Ampicillin	D. Judith
HA-PTP	PTP domain	pDEST-HA	Ampicillin	D. Judith
HA-ARFIP2	ARFIP2	pDEST-HA	Ampicillin	D. Judith
eGFP	Empty	pDEST-eGFP	Ampicillin	T. Johansen
eGFP-PTPMEG2	PTPMEG2	pDEST-eGFP	Ampicillin	D. Judith
eGFP-ARFIP2	ARFIP2	pDEST-eGFP	Ampicillin	D. Judith
eGFP-ARFIP1	ARFIP1	pEGFP-C1	Kanamycin	K. Nakayama

2.5. Data analysis

2.5.1. Western blot quantification

ImageJ (National Institute of Health) densitometry was used for quantification of Western blots. Measurements of signal intensity were transferred to Microsoft Excel for further analysis.

2.5.2. LC3 spots counting

As mentioned previously, the automated counting of LC3 spots was done by the High-Throughput Screening (HTS) facility team at the Francis Crick Institute, using the Opera Phenix High-Content Screening System and its associated Harmony software (PerkinElmer). The raw data collected was then transferred to Microsoft Excel for further analysis.

2.5.3. ATG9A dispersal quantification

ImageJ (National Institute of Health) was used to quantify ATG9A dispersal from the Golgi apparatus (marked by GM130). First, in the GM130 channel, the Golgi area was defined by manually drawing the shape of the GM130-positive staining. Then, in the ATG9A channel, the intensity of the ATG9A staining was measured in this GM130-positiveregion. The same process was repeated with the shape of the whole cell. These ATG9A intensity values were then transferred to Microsoft Excel where the ratio between “Golgi ATG9A” and “Whole cell ATG9A” was calculated.

2.5.4. DNA/protein sequence analysis

DNASTAR (Lasergene) programs were used to analyse nucleotide/amino acid sequence files.

2.5.5. Statistical analysis

The GraphPad Prism 8 software was used for statistical analysis. Details of the statistical tests used are indicated in the legend for each figure. Asterisks indicate significance: * corresponds to $p \leq 0.05$, ** to $p \leq 0.01$, *** to $p \leq 0.001$, and **** to $p \leq 0.0001$.

Chapter 3. Results

3.1. Cell lines, constructs and antibodies

3.1.1. PTPMEG2 CRISPR cell lines

Prior to beginning my thesis, Delphine Judith, a former lab member, generated HEK293A cell lines depleted for PTPMEG2 using the CRISPR-Cas9 genome editing technology [104]. In this thesis, I use two of her control (CTL) cell lines, DCW1 and DCW6, and three of her knock-out (KO) cell lines, FC1.8, FC3.1 and FC3.4. Delphine Judith genotyped them and showed that the expression of PTPMEG2 was lost in the FC1.8, FC3.1 and FC3.4 cell lines due to the introduction of a stop codon in respectively exon 2 and exon 3 of the protein **(Table 3.1)**. These three cell lines are completely deficient of the PTPMEG2 protein, as confirmed by Western blot analysis **(Figure 3.1)**.

Table 3.1: PTPMEG2 CRISPR cell lines. All cell lines were generated and genotyped by Delphine Judith. The PAM sequence is highlighted in bold.

Cell line	Sequence targeted by guide RNA	Outcome	PTPMEG2
DCW1	-	No modification	CTL
DCW6	-	No modification	CTL
FC1.8	5'-ACAATGTTTCCCCGCTGTCT**TGG**-3'	Stop codon in exon 2	KO
FC3.1	5'-**CCA**TAGAATTGTTCCACTCCTAC-3'	Stop codon in exon 3	KO
FC3.4	5'-**CCA**TAGAATTGTTCCACTCCTAC-3'	Stop codon in exon 3	KO

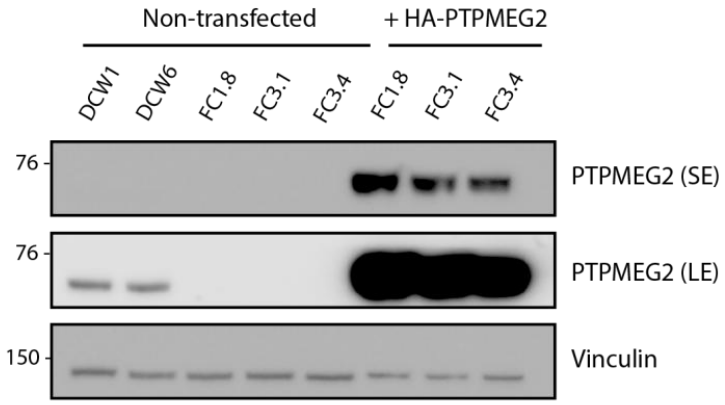

Figure 3.1: PTPMEG2 CRISPR CTL and KO cell lines. HEK293A cells were depleted of PTPMEG2 using the CRISPR-Cas9 technology. DCW1 and DCW6 cell lines are used as control while FC1.8, FC3.1 and FC3.4 are knock-out for PTPMEG2. In the last three lanes, the expression of PTPMEG2 was rescued by transfecting the knock-out cell lines with HA-tagged PTPMEG2. Vinculin was used as a loading control. SE: short exposure, LE: longer exposure.

3.1.2. Subcellular localization of PTPMEG2 and its domains

Delphine Judith also generated constructs in which PTPMEG2 is tagged at its N-terminal end with either HA (hemagglutinin) or eGFP (enhanced green fluorescent protein). The HA tag was also used to label the isolated Sec14 and PTP domains **(Table 2.3)**.

PTPMEG2 is described in the literature as a membrane-associated protein which resides at the surface of secretory vesicles in rat mast cells and Jurkat T cells [82]. This localization on vesicles seems to be due to the Sec14 lipid-binding domain of PTPMEG2 as the isolated Sec14 domain shows a vesicular pattern of expression in the cell while expression of the isolated PTP domain results in a diffuse signal in the cytosol [78]. I decided to check if I could confirm these results when looking at both endogenous PTPMEG2 and at my tagged constructs **(Figure 3.2)**. By doing a crude membrane fractionation assay, I observed that endogenous PTPMEG2 is indeed clearly enriched in the membrane fraction, with a smaller proportion of the protein also found in the cytosol **(Figure 3.2 A)**. ATG9A was used as a control in this assay and was

solely detected in the membrane fraction, as expected. The analysis of HA-tagged PTPMEG2 gave a similar result, with the overexpressed full-length protein mostly found associated to membranes **(Figure 3.2 B)**. Furthermore, the Sec14 domain of PTPMEG2 could only be detected in the membrane fraction, while the PTP domain was clearly expressed in the cytosol, which is in agreement with previous studies.

Altogether, these results confirm that the subcellular localization of our constructs for the full-length PTPMEG2 protein and for its two domains agrees with the published data.

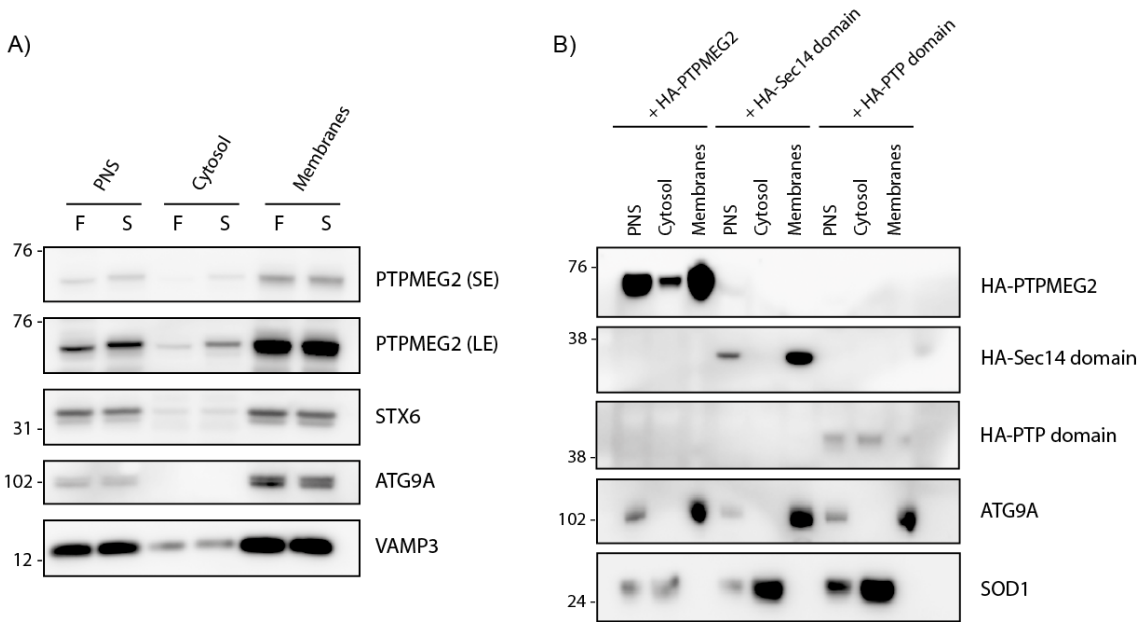

Figure 3.2: Subcellular localization of PTPMEG2 and its isolated domains. Crude membrane fractionation assays were performed to determine the presence of endogenous PTPMEG2 **(A)** or of overexpressed PTPMEG2 and its domains **(B)** either in the cytosol or in the membrane fraction of HEK293A cells. STX6, ATG9A, VAMP3 and SOD1 were used as controls. PNS: Post-nuclear supernatant, F: fed, S: starved, SE: short exposure, LE: longer exposure.

3.1.3. PTPMEG2 antibody generation

The analysis of protein abundance by Western blot and protein localization by immunofluorescence relies on the use of antibodies that are specific for the protein of interest. The commercial antibody for PTPMEG2 that I routinely use in this thesis is the monoclonal mouse IgG_{2B} antibody from R&D Systems, clone #291835 (catalog number: MAB2668). However, although this antibody is useful to detect human PTPMEG2 by Western blot, it does not provide good results when used for immunofluorescence analysis, making it impossible to detect the localization of endogenous PTPMEG2 in my cell lines. Moreover, this antibody is raised against *E. coli*-derived recombinant full-length human PTPMEG2 but the exact epitope recognised and therefore the domain recognised (Sec14 or PTP) were unknown. To solve these two problems, I decided to try to generate my own antibodies against either the Sec14 or the PTP domain of PTPMEG2.

First, I determined the epitopes recognised by the MAB2668 commercial antibody using a peptide array. The peptide array was designed with the help of the Peptide Chemistry facility team at the Francis Crick Institute to cover the full length of PTPMEG2 with peptides of 12 amino acids, each shifted by one amino acid at a time. Two similar arrays were produced. One array was incubated with both the MAB2668 commercial primary antibody and the relevant secondary antibody while the other array was only incubated with the secondary antibody to serve as a negative control. Surprisingly, I found that the MAB2668 antibody binds to two different epitopes, which was unexpected since it is advertised as a monoclonal antibody **(Figure 3.3)**. The first epitope is located in the PTP domain (amino acids 375 to 383), while the second epitope is situated at the very end of the protein sequence (amino acids 582 to 589). This experiment produced valuable information to design immunogenic peptides for the generation of my own antibodies **(Figure 3.4)**. It also demonstrated that the MAB2668 commercial antibody is not suitable to detect the isolated Sec14

domain of PTPMEG2 and can only be used to detect the isolated PTP domain or the full-length protein.

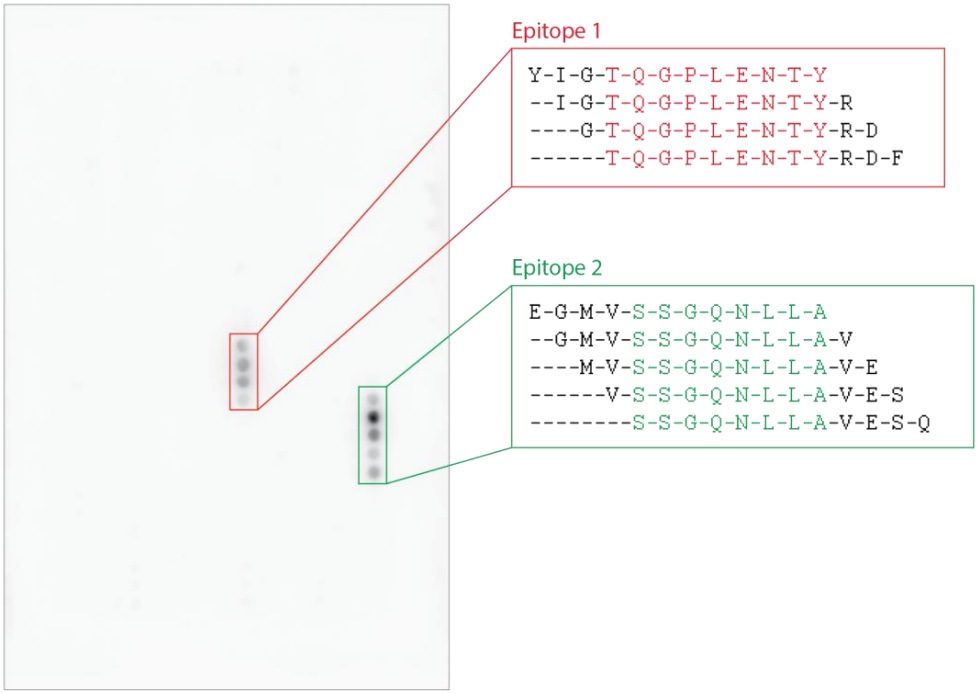

Figure 3.3: Epitope mapping of the R&D MAB2668 antibody. A peptide array membrane covering the full length of PTPMEG2 was incubated with the MAB2668 primary antibody then with an HRP-conjugated anti-mouse secondary antibody. Two epitopes were detected: the first one (red) is located in the PTP domain of PTPMEG2 (amino acids 375 to 383), while the second one (green) is situated at the end of the protein sequence (amino acids 582 to 589).

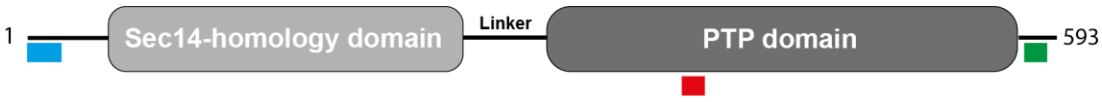

Figure 3.4: Epitopes recognized by my PTPMEG2 immunogenic peptides. Two sets of peptides were used in an effort to produce homemade PTPMEG2 rabbit polyclonal antibodies. One peptide corresponding to the first 20 amino acids of PTPMEG2 was generated in order to raise antibodies against the N-terminal end of the protein (blue) in rabbits #1113 and #1114, while a mix of two peptides corresponding to amino acids 375-383 (red) and 582-589 (green) was used to immunize rabbits #1115 and #1116 against the C-terminal end of PTPMEG2.

With this information in mind and again with the help of the Peptide Chemistry facility team, peptides from the PTPMEG2 amino acid sequence were designed and produced to serve as immunogens for the generation of my own rabbit polyclonal antibodies. I aimed to generate two antibodies: one directed against the N-terminal portion of PTPMEG2 and the other raised against the C-terminal portion, in order to be able to study both the Sec14 and PTP domains independently. The first 20 amino acids of the PTPMEG2 sequence were used for the N-terminal peptide, while the epitopes found with the peptide array experiment served as the C-terminal peptides **(Figure 3.4)**. All these peptides were sent to Pettingill Technology who performed the immunization of the rabbits. Two rabbits (#1113 and #1114) were immunized with the N-terminal peptide (amino acids 1-20 of PTPMEG2) to generate antibodies for the Sec14 domain, and two other rabbits (#1115 and #1116) were immunized with the C-terminal peptides mix (amino acids 375-386 and 581-592 of PTPMEG2) to generate antibodies against the PTP domain.

The pre-immune serum was collected for all four rabbits prior to immunization, followed by the harvest of the serum at 4 different time points through the immunization process (Bleeds 1, 2, 3 and 4). Upon reception of every new set of sera, I tested each serum against lysates obtained from DCW1 control cells (to detect endogenous PTPMEG2), from FC1.8 knock-out cells (to check the absence of PTPMEG2) and from FC1.8 cells overexpressing HA-tagged PTPMEG2 (to detect the rescued overexpression of PTPMEG2) **(Figure 3.5)**. The pre-immune serum was also tested to assess background staining and the commercial MAB2668 antibody was included to serve as a positive control. Towards the reception of the third bleed, all four sera could detect the overexpressed PTPMEG2 but only the sera from rabbits #1113 and #1114 were clean enough to show the absence of PTPMEG2 in the knock-out cell line and its presence in the control cell line. Unfortunately, due to a mistake made by Pettingill Technology, the final bleed from these two rabbits was lost, only leaving the third bleed to use for Western blot detection of the Sec14 domain of PTPMEG2. On the other hand, none of the bleeds obtained from rabbits #1115

and #1116 seemed suitable for Western blot detection of the PTP domain of PTPMEG2 as all of them gave a dirty signal and a band in the knock-out sample. However, as mentioned previously, the MAB226 commercial antibody can be used to detect the PTP domain.

All these sera were also tested for immunofluorescence detection of PTPMEG2 but unfortunately none of them allowed me to visualize the endogenous protein. For this reason, all the analysis done on the localization of PTPMEG2 during this project relied on the use of eGFP-tagged constructs.

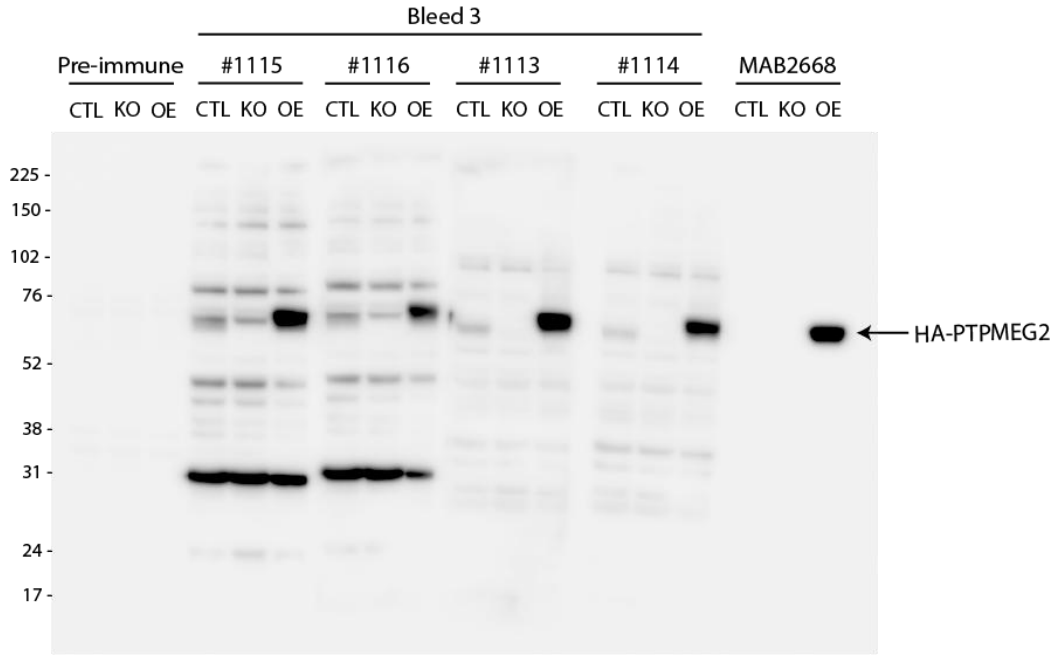

Figure 3.5: PTPMEG2 antibody generation (third bleed test). The serum of each immunized rabbit (#1115, 1116, 1113 and 1114) was tested against lysates generated from DCW1 cells (CTL), FC1.8 cells (KO) or FC1.8 cells overexpressing HA-PTPMEG2 (OE). The pre-immune serum from rabbit #1113 was included to assess the background staining and the MAB2668 commercial antibody was included as a positive control.

3.2. Impact of PTPMEG2 on autophagosome formation

Since PTPMEG2 is found on ATG9A-positive membranes, the first question I wanted to address was whether or not PTPMEG2 could regulate the autophagic process. To test this, I looked at the lipidation of LC3 by Western blot and immunofluorescence. LC3-II (or lipidated LC3) is often used as an indicator of autophagosome formation and remains the “gold standard” in the field to investigate the effect of a potential regulator on autophagy.

First, I assessed the efficiency of LC3 lipidation in all my cell lines by Western blot **(Figure 3.6)**. Each of the two control cell lines was compared to all three PTPMEG2 knock-out cell lines in fed, starved and bafilomycin A1-treated conditions. Bafilomycin A1 treatment interferes with the fusion between autophagosomes and lysosomes and therefore results in an accumulation of closed autophagosomes. It is often used to discriminate whether a potential regulator of autophagy acts in the early steps of the pathway or later, at the stage of autophagosome-lysosome fusion or degradation. After quantification of the LC3-II/vinculin ratio, this experiment revealed that the absence of PTPMEG2 does not seem to affect LC3 lipidation as no statistical difference was noted between the control and knock-out cell lines.

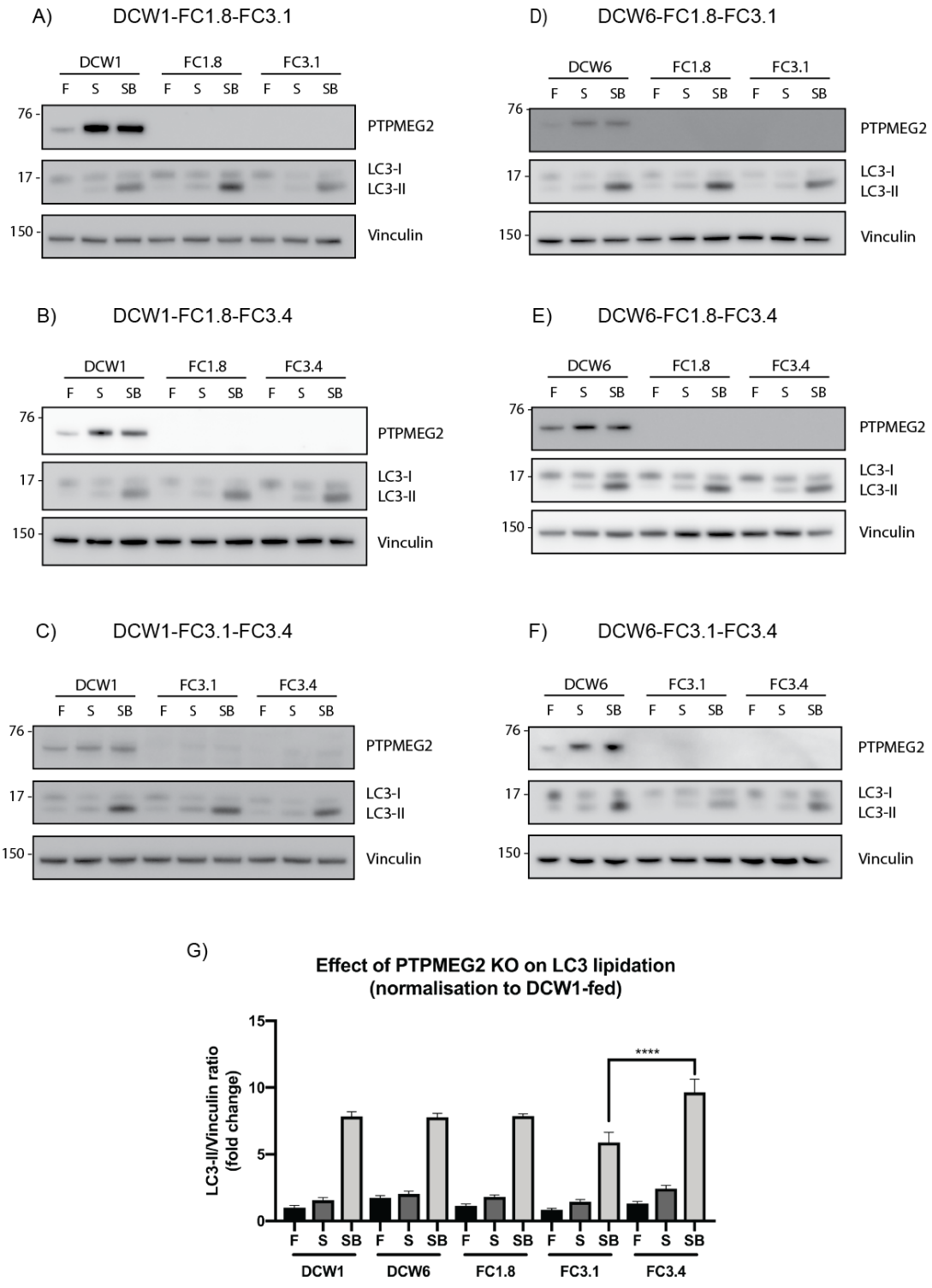

Figure 3.6: Impact of PTPMEG2 KO on LC3 lipidation. A-F) The lipidation of LC3 was assessed for each of the PTPMEG2 CTL and KO cell lines in fed (F), starved (S) and starved and bafilomycin A1-treated (SB) conditions. Each blot was done twice. Vinculin was used as a loading control. **G)** The average of LC3-II/vinculin ratio was calculated for each cell line, with DCW1-fed acting as reference and normalized to 1 and the rest of the values normalized to it. The graph represents the mean with SEM, with a one-way ANOVA and Tukey's post-test analysis. No statistical difference was found between the CTL and KO cell lines.

Following this, I decided to confirm this result by looking at LC3 spots formation by immunofluorescence. As depicted in **Figure 3.7 A**, starvation resulted in the appearance of LC3-positive structures in the cytosol of both PTPMEG2 control and knock-out cells. As expected, the number of these structures further increased when cells were treated with bafilomycin A1 and this increase was not impaired either by the absence of PTPMEG2 in the knock-out cells. In an effort to quantify the number of spots in an unbiased way, I collaborated with the High-Throughput Screening (HTS) facility team at the Francis Crick Institute. PTPMEG2 control and knock-out cells were plated in 24-well, clear-bottom microplates that were then imaged and analysed using the Opera Phenix High-Content Screening System and the associated Harmony software. The result of this analysis is shown in **Figure 3.7 B**. Consistently with what I observed by Western blot, no difference was noted in the formation of LC3 spots between PTPMEG2 control and knock-out cell lines.

Taken together, these results suggest that PTPMEG2 is not involved in LC3 lipidation and therefore, that it probably does not regulate autophagosome formation.

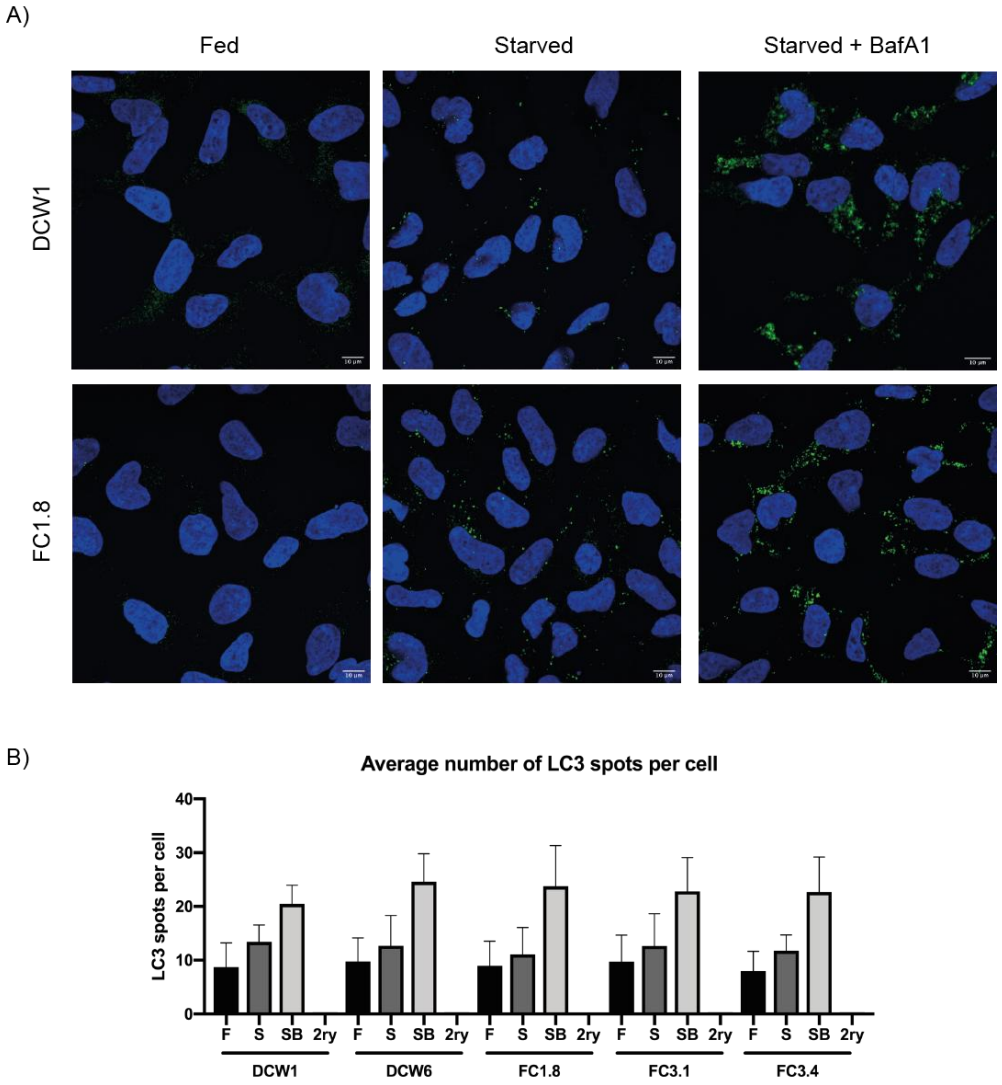

Figure 3.7: Impact of PTPMEG2 KO on LC3 spots formation. PTPMEG2 CTL and KO cell lines were stained for LC3 and the average number of LC3-positive spots formed was assessed in fed (F), starved (S) and starved and bafilomycin A1-treated (SB) conditions by confocal microscopy. Representative pictures acquired manually are shown in **A** (scale bar: 10 µm). To quantify the number of spots in an unbiased way, pictures were also acquired and analysed using the Opera Phenix High-Content Screening System and the associated Harmony software with the help of the High-Throughput Screening facility team at the Francis Crick Institute **(B)**. This analysis was performed just twice and therefore requires to be repeated. A secondary antibody-only (2ry) condition was used as a negative control. The graph represents the mean with SEM, with a one-way ANOVA and Tukey's post-test analysis. No statistical difference was found between the CTL and KO cell lines.

3.3. Relationship between PTPMEG2 and ATG9A

Given its presence on ATG9A-positive membranes, I decided to investigate whether PTPMEG2 could play a role in ATG9A function or trafficking.

First, I looked at the protein level of ATG9A in the presence or absence of PTPMEG2. Western blot analysis showed no difference between PTPMEG2 control and knock-out cells, in both fed and starved conditions **(Figure 3.8)**.

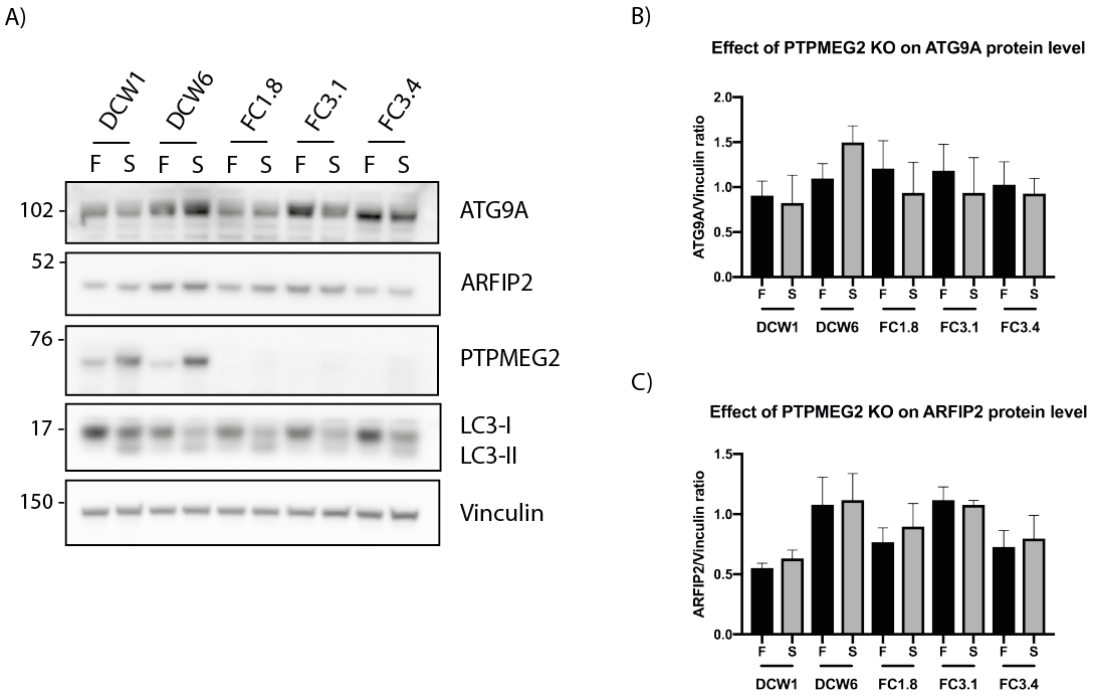

Figure 3.8: Impact of PTPMEG2 KO on ATG9A and ARFIP2 protein level. A) PTPMEG2 CTL and KO cells were either fed (F) or starved (S) for 2 hours prior to lysis. Vinculin was used as a loading control. This experiment was done three times. **B-C)** The average of ATG9A/vinculin ratio and ARFIP2/vinculin ratio was calculated for each cell line. The graph represents the mean with SEM, with a one-way ANOVA and Tukey's post-test analysis. No statistical difference was found between the CTL and KO cell lines.

I then decided to investigate if PTPMEG2 could somehow regulate the trafficking of ATG9A. ATG9A is indeed known to localize on the Golgi apparatus in fed conditions and to disperse in the cytosol upon starvation [43]. To visualize and quantify this dispersal, PTPMEG2 control and knock-out cells were stained for ATG9A and GM130 and were either kept in full medium or deprived of amino acids for 2 hours **(Figure 3.9)**. As expected, in control cells, ATG9A strongly colocalized with GM130 in fed conditions but was found diffuse in the cytosol in starved cells. However, in PTPMEG2 knock-out cells, this dispersal phenotype was already observed in fed conditions, with the ATG9A signal being less enriched on the Golgi and more diffuse in the cytosol **(Figure 3.9 A)**. The dispersal of ATG9A was quantified by calculating the ratio between the ATG9A signal intensity on the Golgi (i.e. in the GM130-positive area) and in the whole cell. This quantification indicated that in the absence of PTPMEG2 the reduction of ATG9A colocalization with GM130 and its concomitant dispersal in the cytosol were significant **(Figure 3.9 B)**.

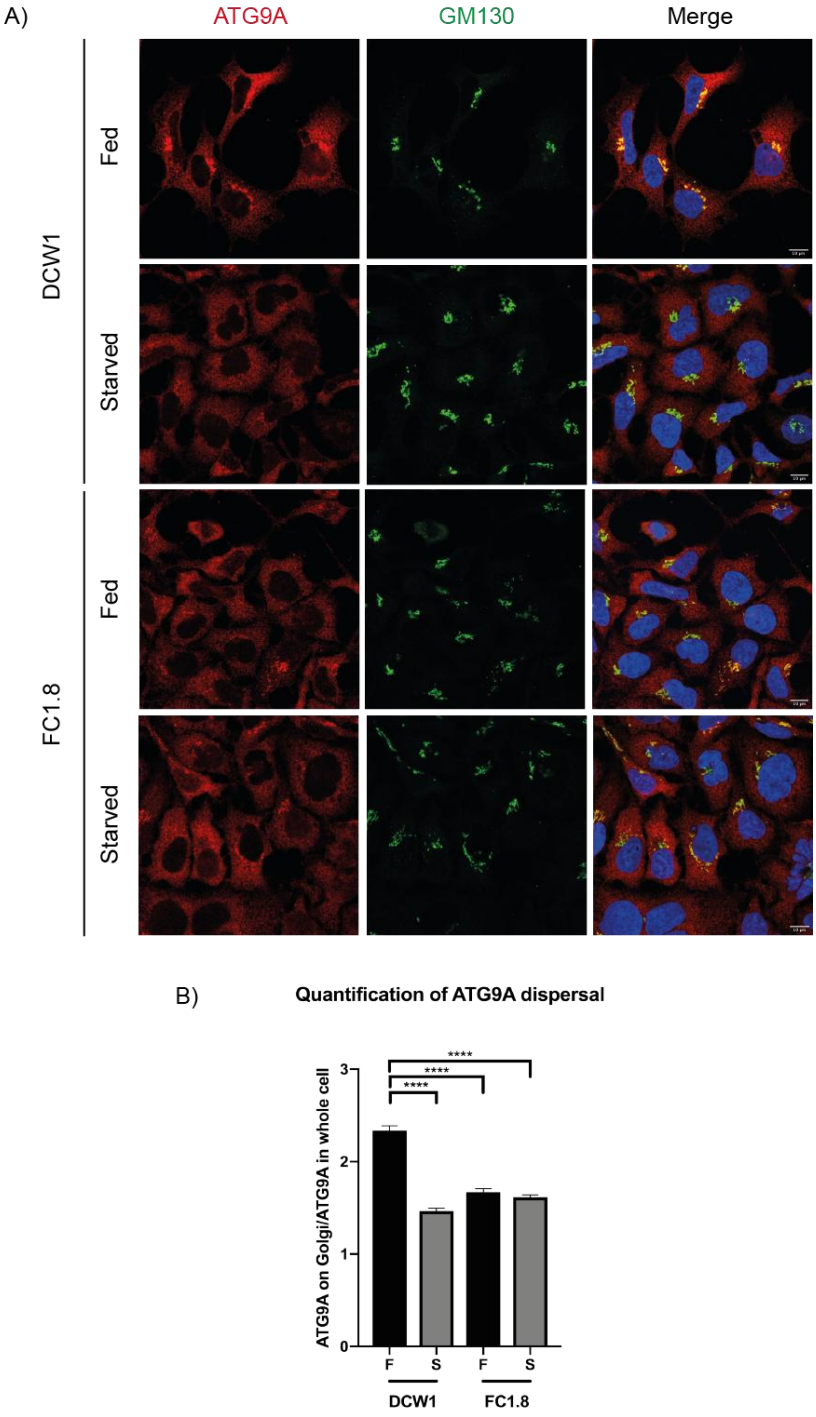

Figure 3.9: Impact of PTPMEG2 KO on ATG9A localization. PTPMEG2 CTL and KO cell lines were either fed (F) or starved (S) for 2 hours and stained for ATG9A and GM130 to look at the dispersal of ATG9A from the Golgi. Pictures were acquired manually by confocal microscopy **(A)** (scale bar: 10 µm). The ATG9A dispersal was then quantified by calculating the ratio between the ATG9A signal intensity on the Golgi and in the whole cell **(B)**. This experiment was done three times with the quantification done in 50 cells for each condition in each experiment. The graph represents the mean with SEM, with a one-way ANOVA and Tukey's post-test analysis.

These results suggest that PTPMEG2 might be involved in the regulation of the trafficking of ATG9A. The absence of PTPMEG2 seems to result in a more dispersed, cytosolic localization of ATG9A similar to what is normally observed in starved conditions. Interestingly, the same phenotype is observed upon ARFIP2 knock-out. However, it is worth noting that the overexpression of eGFP-tagged PTPMEG2 did not have any effect on the localization of ATG9A in a preliminary experiment (data not shown). Therefore, the evidence for an impact of PTPMEG2 on ATG9A trafficking needs to be strengthened.

Finally, since PTPMEG2 was previously found associated to the ATG9A-positive compartment, I wanted to assess whether PTPMEG2 and ATG9A could interact. Using my commercial PTPMEG2 antibody coupled to Protein G magnetic beads, I pulled-down endogenous PTPMEG2 and looked for the presence of endogenous ATG9A. Despite the relatively low efficiency of the immunoprecipitation (PTPMEG2 was only slightly enriched), I could clearly detect ATG9A in the IP fraction, in both fed and starved conditions **(Figure 3.10)**.

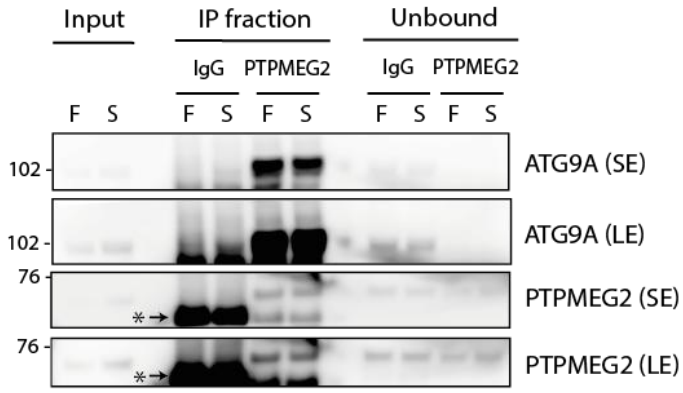

Figure 3.10: Interaction between endogenous PTPMEG2 and ATG9A. HEK293A cells were either fed (F) or starved (S) for 2 hours prior to lysis. Immunoprecipitation (IP) of endogenous PTPMEG2 was performed using Protein G magnetic beads coupled to PTPMEG2 antibody (or to purified mouse IgG as a control) and membranes were later blotted with anti-ATG9A and anti-PTPMEG2 antibodies. The asterisk (*) indicates the mouse IgG heavy chain. This experiment was done twice. SE: short exposure, LE: longer exposure.

Altogether, these results seem to indicate that PTPMEG2 and ATG9A interact and that PTPMEG2 might have a function in the regulation of ATG9A trafficking.

3.4. Relationship between PTPMEG2 and ARFIP2

ARFIP2 is a BAR domain-containing protein which, like PTPMEG2, was found enriched on ATG9A-positive membranes. Its knock-out leads to a clear dispersal of ATG9A from the Golgi to the cytosol in fed conditions [60], the same phenotype I seem to observe in my PTPMEG2 knock-out cells. For these reasons, I decided to explore the link between PTPMEG2 and ARFIP2 in the context of autophagy.

To start with, I looked at the potential impact of PTPMEG2 knock-out on the protein level of ARFIP2. However, Western blot analysis showed no difference between the PTPMEG2 control and knock-out cell lines **(Figure 3.8)**.

I then investigated whether PTPMEG2 could influence the localization of ARFIP2. PTPMEG2 control and knock-out cell lines were either fed or starved, and stained for ARFIP2 and GM130 **(Figure 3.11)**. As expected, ARFIP2 was found enriched on the Golgi apparatus (as marked by GM130) in both fed and starved conditions, but the absence of PTPMEG2 did not seem to alter its localization.

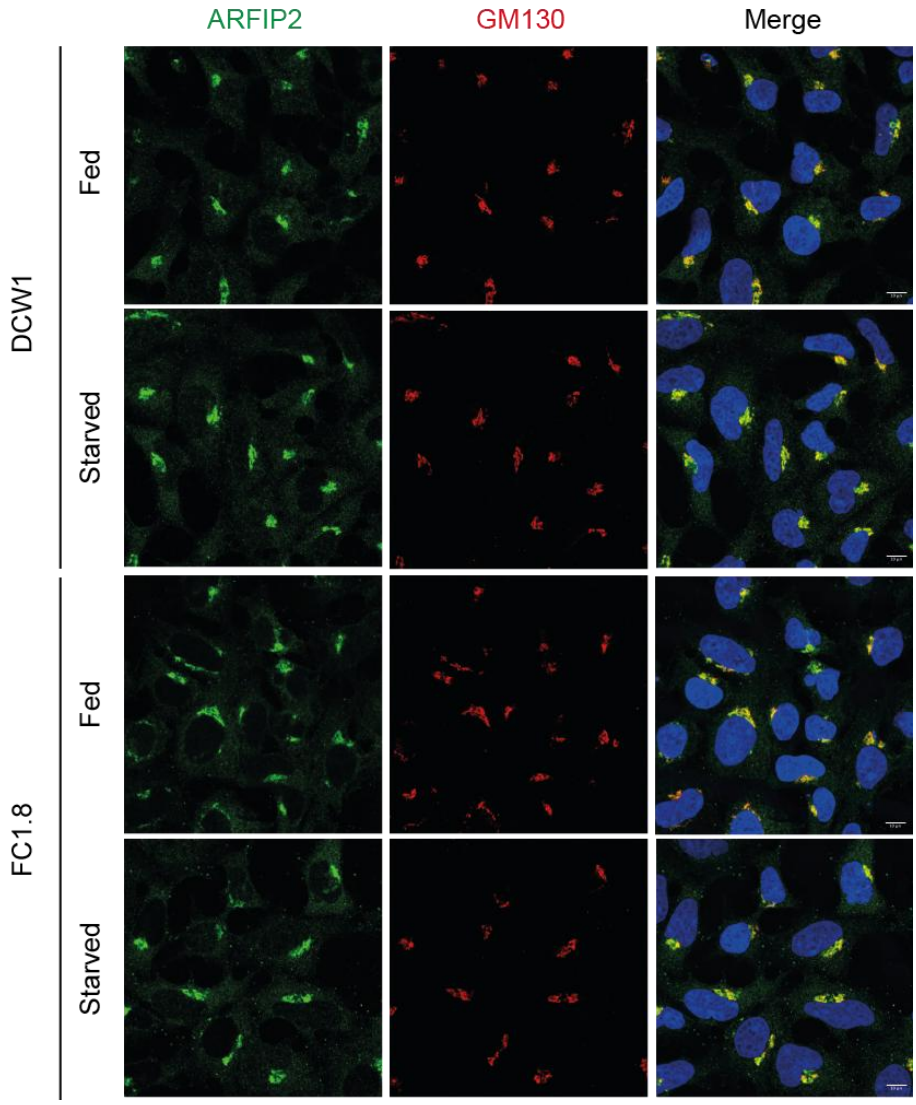

Figure 3.11: Impact of PTPMEG2 KO on ARFIP2 localization. PTPMEG2 CTL and KO cell lines were either fed (F) or starved (S) for 2 hours and stained for ARFIP2 and GM130. Pictures were acquired manually by confocal microscopy (scale bar: 10 µm).

Interestingly, a link between PTPMEG2 and ARFIP2 has previously been reported in the literature. Saito *et al.* indeed reported a strong interaction between the N-terminal portion of PTPMEG2 and ARFIP2 [78]. Therefore, I aimed to test if I could observe this interaction between ARFIP2 and PTPMEG2 full-length. Using GFP-TRAP beads, I pulled-down eGFP-tagged PTPMEG2 and checked if I could detect the presence of HA-tagged ARFIP2 in the immunoprecipitate (IP) **(Figure 3.12)**. I found that HA-ARFIP2 was indeed

detectable in the IP fraction upon overexpression of eGFP-PTPMEG2 but not upon co-expression of the eGFP empty vector, suggesting that ARFIP2 is probably associated with PTPMEG2 full-length, either directly or indirectly.

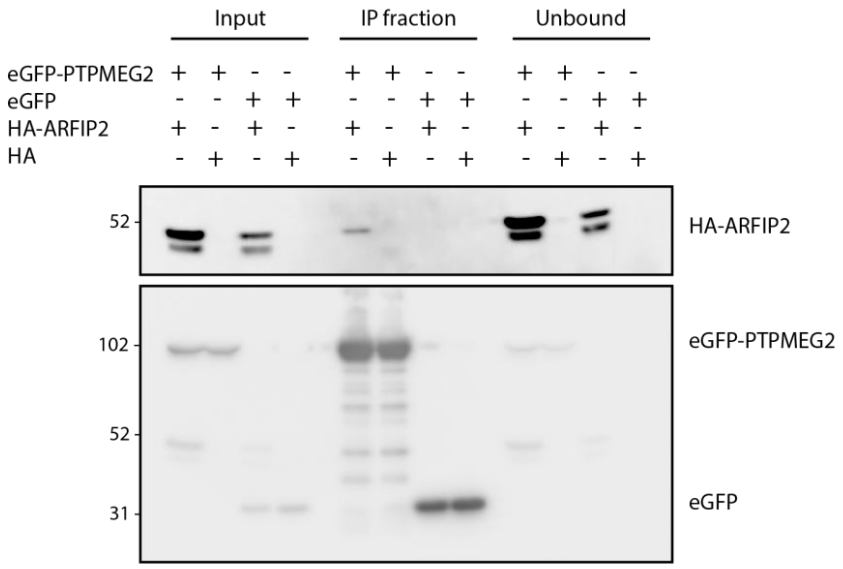

Figure 3.12: Interaction between eGFP-PTPMEG2 and HA-ARFIP2. HEK293A cells were co-transfected with either eGFP-PTPMEG2 or the associated eGFP empty vector, and HA-ARFIP2 or the associated HA empty vector. Immunoprecipitation (IP) was performed using GFP-TRAP beads and membranes were later blotted with anti-HA and anti-GFP antibodies. This experiment was done twice.

Afterwards, I decided to check if PTPMEG2 could also interact with ARFIP1, another protein of the Arfaptin family that Delphine Judith also found associated to ATG9A-positive membranes. This time, I immunoprecipitated eGFP-tagged ARFIP1 and ARFIP2 using GFP-TRAP beads and looked for the presence of HA-tagged PTPMEG2 in the IP fraction **(Figure 3.13)**. I found that PTPMEG2 was associated with ARFIP2 but also with ARFIP1 and that the interaction with ARFIP1 actually seemed much stronger than the one with ARFIP2. However, this result needs confirmation as this experiment was performed only once.

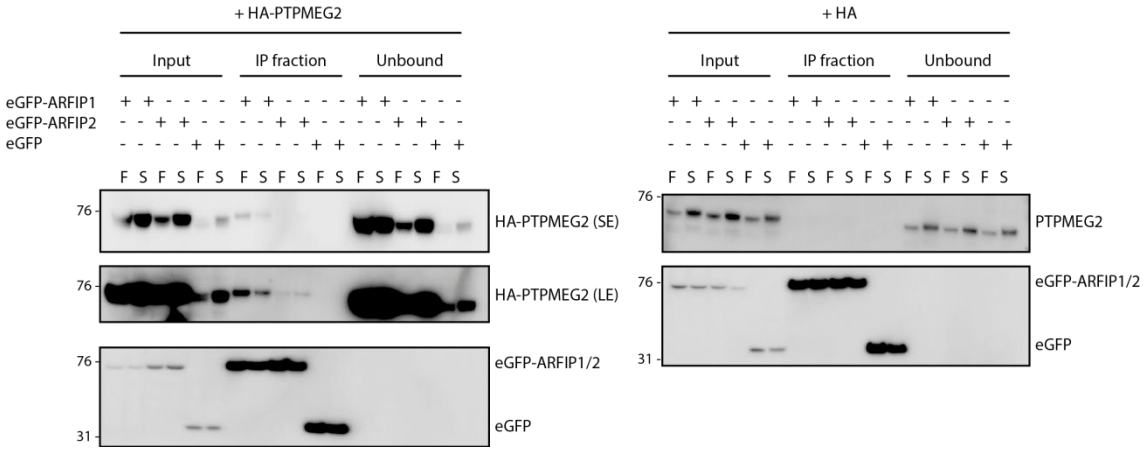

Figure 3.13: Interaction between eGFP-ARFIP1, eGFP-ARFIP2 and HA-PTPMEG2. HEK293A cells were co-transfected with either eGFP-ARFIP1, eGFP-ARFIP2 or the associated eGFP empty vector, and HA-PTPMEG2 or the associated HA empty vector. Immunoprecipitation (IP) was performed using GFP-TRAP beads and membranes were later blotted with anti-HA, anti-GFP and anti-PTPMEG2 antibodies. This experiment was done once. F: fed, S: starved.

These results indicate that PTPMEG2 and ARFIP2 seem to interact in both fed and starved conditions. However, the significance of this interaction is still unknown as I could not observe any impact of the absence of PTPMEG2 on the protein level or on the localization of ARFIP2. Likewise, preliminary results I obtained did not indicate any major mislocalization of PTPMEG2 in ARFIP2 KO cells (data not shown). Therefore, the nature of the relationship between PTPMEG2 and ARFIP2 and its role in the context of ATG9A function remain to be established.

Chapter 4. Discussion

Autophagy is a complex process whose completion relies on the interplay of multiple actors in a timely and spatially ordered fashion. In addition to the core machinery of ATG proteins, phospholipids, accessory proteins and regulators play a big part in the pathway and are increasingly studied. In this thesis, I investigated the putative involvement of the tyrosine phosphatase PTPMEG2 in mammalian autophagy and ATG9A function.

Amongst the ATG proteins so far identified, ATG9A remains the one we least understand as its exact function is still unclear. Our group previously demonstrated that ATG9A localizes at the TGN in fed conditions but disperses in the cytosol in the form of ATG9A-positive vesicles upon starvation [43]. These vesicles seem to briefly interact with forming autophagosomes then cycle back to the Golgi upon refeeding [42, 43]. This suggests that ATG9A vesicles could promote phagophore expansion at the ER by supplying lipids or proteins from other compartments. In an effort to test this hypothesis, a former member of our laboratory, Delphine Judith, immunoisolated ATG9A-positive vesicles and analysed their protein content [60]. This experiment revealed the presence of PTPMEG2 on ATG9A-positive membranes. Since this protein tyrosine phosphatase had never been described in the context of autophagy before, I aimed to investigate whether PTPMEG2 could be a potential new regulator of the autophagic response and if it could somehow be involved in the function or trafficking of ATG9A.

First, I explored the impact of the absence of PTPMEG2 on the autophagic response, using PTPMEG2 CRISPR KO cell lines generated by Delphine Judith. To assess whether the formation of autophagosomes was affected, I looked at the lipidation of LC3 by Western blot and at the formation of LC3-positive spots by immunofluorescence. The Western blot analysis revealed that the absence of PTPMEG2 did not seem to impair LC3 lipidation as no significant difference in the levels of LC3-II was noted between PTPMEG2 CTL and KO cell lines.

The number of LC3 spots formed was assessed by high-throughput screening to allow for unbiased, automatic spots counting. This experiment demonstrated that the number of LC3-positive spots formed was similar in PTPMEG2 CTL and KO cell lines. These two experiments were done in fed, starved, and starved and bafilomycin A1-treated conditions, and indicated that PTPMEG2 does not seem to be involved in the generation of LC3-positive autophagosomes. However, it is worth noting that LC3 acts relatively late in the autophagic pathway. Therefore, it would be interesting to analyse the impact of PTPMEG2 loss on the formation of earlier structures such as ULK1, WIPI2 or ATG16L1 spots formation.

There are at least two other reasons to investigate earlier autophagic structures. First, as PTPMEG2 was found associated to ATG9A vesicles and ATG9A seems to be involved in the initial recruitment of the ULK complex to the ER [41, 60], it could be informative to assess whether the loss of PTPMEG2 impairs this very early event in the pathway.
Second, a link between PTPMEG2 and the VPS34 complex might exist. It has indeed been demonstrated that PTPMEG2 can dephosphorylate EGFR [88] and EGFR itself has been shown to phosphorylate Beclin1, which leads to a reduced binding of Beclin1 to VPS34 [105]. Moreover, PTPMEG2-positive vesicles have been reported to also be positive for VPS34 [74]. Next, VPS34 is known to be phosphorylated on at least two tyrosine residues that are important for its trafficking [106]. As PTPMEG2 is a tyrosine phosphatase, it could potentially target these sites. Finally, UVRAG has also been linked to ATG9A dispersal [50]. Therefore, a potential involvement of PTPMEG2 in the function or recruitment of the VPS34 complex might be worth exploring.

After examining the formation of autophagosomes, I decided to focus on the relationship between PTPMEG2 and ATG9A as PTPMEG2 was found enriched on immunoisolated ATG9A-positive membranes [60].

I started by assessing whether the absence of PTPMEG2 would affect the protein abundance of ATG9A. However, there seemed to be no significant difference in the level of ATG9A between PTPMEG2 CTL and KO cell lines, as seen by Western blot.

Then, I looked at a possible effect of PTPMEG2 KO on the localization of endogenous ATG9A. While the localization of ATG9A was as expected in control cells (i.e. Golgi-localized in fed conditions and dispersed after 2 hours of starvation), the absence of PTPMEG2 seemed to lead to an increased ATG9A dispersal in fed cells. Interestingly, this phenotype mimics the behaviour of ATG9A observed in ARFIP2 KO cells [60]. However, this dispersal effect needs to be confirmed as the overexpression of eGFP-tagged PTPMEG2 in cells did not appear to affect ATG9A localization. Moreover, I could consistently observe a strong impact of both PTPMEG2 knock-out and PTPMEG2 overexpression on the Golgi morphology. The Golgi apparatus, which normally appears relatively compact with confocal microscopy, frequently looked more fragmented whenever the expression of PTPMEG2 was modulated. This could be explained by the fact that PTPMEG2 is known to promote fusion events [81] and such events are crucial in the maintenance of the Golgi structure and compartmentalization. This altered Golgi morphology made the assessment of ATG9A dispersal difficult at times. It is also possible that this abnormal Golgi structure could impact its function and therefore interfere with the normal trafficking of proteins, such as ATG9A.

Finally, I investigated whether PTPMEG2 and ATG9A could interact. After pulling-down endogenous PTPMEG2 I could detect ATG9A in the immunoprecipitate in both fed and starved conditions, indicating the two proteins are associated. Since they interact, one hypothesis is that PTPMEG2 could dephosphorylate ATG9A to modulate its activity, its localization or its binding to other proteins. One potentially interesting residue to examine in this direction is Tyr8, as ATG9A has been described to be phosphorylated on this residue by the Src kinase [57]. This phosphorylation is thought to be constitutive

and to promote ATG9A trafficking between the TGN, the plasma membrane and endosomes. In addition to Tyr8, ATG9A could be phosphorylated on other tyrosine residues that would potentially be worth studying as well.

Finally, in the last results section, I tried to better understand the link between PTPMEG2 and ARFIP2 since both proteins are found associated to the immunoisolated ATG9A compartment and their depletion seems to cause ATG9A dispersal in fed conditions.

First, I looked at the protein level of ARFIP2 in PTPMEG2 CTL and KO cells. However, as for ATG9A, the absence of PTPMEG2 did not cause any change in the abundance of ARFIP2. Furthermore, the analysis of the localization of ARFIP2 by immunofluorescence did not reveal any impact of PTPMEG2 KO, with ARFIP2 being clearly enriched on the Golgi in both PTPMEG2 CTL and KO cell lines.

Afterwards, I tested if PTPMEG2 and ARFIP2 could interact. An interaction between Flag-tagged ARFIP2 and the HA-tagged Sec14 domain of PTPMEG2 had previously been demonstrated in Jurkat T cells [78]. I showed that eGFP-PTPMEG2 full-length could interact with HA-ARFIP2 in HEK293A cells, as seen by coimmunoprecipitation with GFP-TRAP beads. The reverse immunoprecipitation of eGFP-ARFIP2 later confirmed this association with HA-PTPMEG2 in fed and starved conditions. In this experiment, I could also observe an interaction between HA-PTPMEG2 and eGFP-ARFIP1, although this would need to be confirmed as this assay was done just once. As ARFIP1 and ARFIP2 share a high degree of similarity in their C-terminal portion (which contains a BAR domain and an amphipathic helix), it is quite likely that PTPMEG2 might interact with that region, which would explain why it binds to both proteins.

Regarding the meaning of the interaction between PTPMEG2 and ARFIP2, the data I collected does not allow me to make any firm conclusion. However, as

discussed in the hypothetical model, one possible function of ARFIP2 could be to recruit PTPMEG2 on ATG9A-positive membranes, either directly or indirectly, or to promote the generation of PI4P on these membranes [60], with PI4P binding and activating PTPMEG2 [72]. However, these are only speculations at this point and more experiments are needed to better understand the relationship between PTPMEG2 and ARFIP2, and its relevance in the context of ATG9A function.

Although the results I obtained in this thesis are not sufficient to draw a definitive picture of the role of PTPMEG2 in the context of autophagy, one hypothesis I derived from my data would be that PTPMEG2 could possibly help in the recapture of ATG9A vesicles at the Golgi level. Our group previously demonstrated that ATG9A vesicles could indeed cycle back to the Golgi apparatus [43] and my own results seem to indicate that the loss of PTPMEG2 appears to lead to an increased dispersal of ATG9A. This dispersal could result from either an increased budding of ATG9A vesicles from the Golgi or a reduced recapture. Given the fact that PTPMEG2 has clearly been established to promote fusion events [81], my guess is that PTPMEG2 is more likely to facilitate recapture rather than enhance fission in this context, but this obviously would need to be confirmed.

Therefore, I suggest the following hypothetical model **(Figure 4.1)**. In this model, PTPMEG2 and ARFIP2 interact and are both associated to the membranes of the TGN and of ATG9A vesicles, as demonstrated by their localization as seen by immunofluorescence and by the proteomic analysis of the immunoisolated ATG9A compartment previously realised by Delphine Judith [60]. Although the significance of the interaction between PTPMEG2 and ARFIP2 is still unclear, two hypotheses can be considered. First, the role of ARFIP2 could be to help recruit PTPMEG2 on ATG9A-positive membranes. One study indeed suggested that some vesicle-trafficking proteins might help target PTPMEG2 to its subcellular localization on secretory vesicles by interacting with its Sec14 domain [78]. A second possibility is that ARFIP2 might be important to promote

PI4P generation on ATG9A-positive membranes and PTPMEG2 could be recruited through its binding to PI4P. This is supported by the observation that the loss of ARFIP2 leads to a reduced level of PI4KIIα and PI4KIIIβ on ATG9A membranes [60] and by the demonstrated binding of PTPMEG2 to PI4P [74, 75], respectively. Then, once bound to PI4P, the Sec14 domain of PTPMEG2 could activate the PTP domain [72] and the activated PTPMEG2 could thus potentially dephosphorylate its substrate NSF [81] to promote the fusion of ATG9A vesicles back to the Golgi.

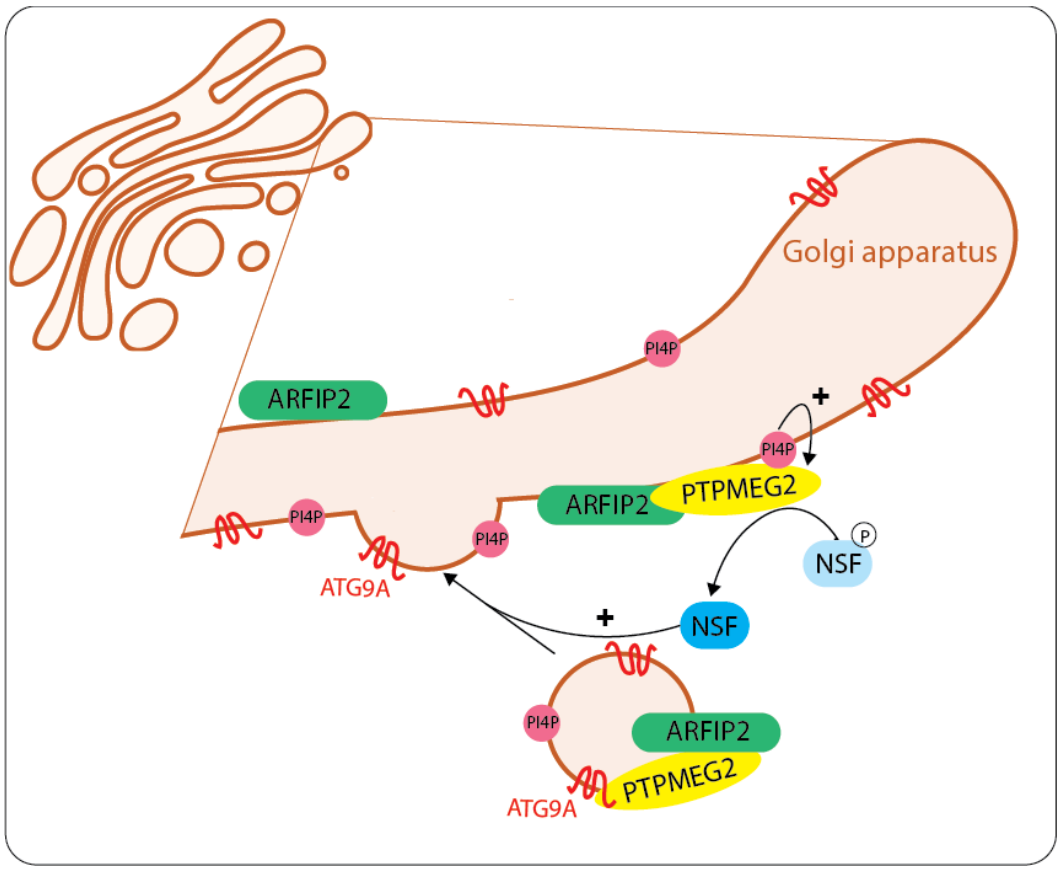

Figure 4.1: Hypothetical model. Based on the data presented in this thesis and on the information provided by existing publications, a possible function of PTPMEG2 could be to facilitate the recapture of ATG9A vesicles at the TGN by promoting the fusion of the vesicles with the Golgi membrane. However, this model is highly hypothetical and many more experiments are needed to confirm or reject it.

However, as mentioned before, this model is by no means an absolute certainty as it is only based on the preliminary data I generated and on information I gathered from the literature. Many aspects of the model need to be confirmed

or further investigated, while others (such as the involvement of NSF in the recapture) are purely speculative. It is nevertheless one possible hypothesis for the function of PTPMEG2 on ATG9A-positive membranes that might be worth exploring in the future.

To conclude this thesis, I would like to suggest some follow-up experiments to improve both our general knowledge of PTPMEG2 (as the literature on this protein is quite limited) and our understanding of its role in autophagy.

First, this project was made challenging by the lack of a good antibody to visualize the localization of endogenous PTPMEG2 by immunofluorescence. As explained earlier, my attempt to generate my own antibody was unfortunately unsuccessful and I had to rely on the overexpression of eGFP-tagged PTPMEG2 for immunofluorescence experiments, which is not ideal as the overexpression of proteins can cause artefacts. To overcome these difficulties, it would be useful to make use of the CRISPR-Cas9-mediated protein tagging method which enables researchers to express fluorescently-tagged proteins at endogenous levels [107]. Once PTPMEG2 can be visualized, its colocalization with different autophagy actors and its response to different conditions can be assessed, which should be informative.

Next, as the reason for the presence of PTPMEG2 on ATG9A vesicles is still unclear, it would be very interesting to repeat the analysis of the protein content of the immunoisolated vesicles (as previously done by Delphine Judith [60]) in the context of PTPMEG2 CTL and KO cell lines. A phosphoproteomics analysis should be coupled to this experiment to add an additional level of information. It is interesting to note that PTPMEG2-positive vesicles have also been reported to be positive for PI4KIIIβ [74]. The presence of this kinase on ATG9A vesicles might therefore be affected by the absence of PTPMEG2, as well as the presence of other key actors of autophagy.

Then, if the ATG9A dispersal phenotype in PTPMEG2 KO cells is confirmed, an investigation of the link between PTPMEG2 and other regulators of ATG9A trafficking (AP complexes, TRAPPIII complex, etc) should be done.

Finally, to gain more insight into the role of PTPMEG2 in and outside of autophagy, it might be worth taking advantage of the BioID technology to identify new substrates and interactors of the protein [108, 109]. This can be done in a variety of conditions depending of the question asked (untreated HEK293A cells, fed *versus* starved conditions, ARFIP2 CTL *versus* KO cells, etc). Similarly, a global phosphoproteomics analysis of tyrosine residues in PTPMEG2 CTL and KO cells could also generate information on potential new substrates.

Reference List

1. Li, W.W., J. Li, and J.K. Bao, *Microautophagy: lesser-known self-eating.* Cell Mol Life Sci, 2012. **69**(7): p. 1125-36.
2. Kaushik, S. and A.M. Cuervo, *The coming of age of chaperone-mediated autophagy.* Nat Rev Mol Cell Biol, 2018. **19**(6): p. 365-381.
3. Mizushima, N., et al., *Autophagy fights disease through cellular self-digestion.* Nature, 2008. **451**(7182): p. 1069-75.
4. Mizushima, N. and M. Komatsu, *Autophagy: renovation of cells and tissues.* Cell, 2011. **147**(4): p. 728-41.
5. Mercer, T.J., A. Gubas, and S.A. Tooze, *A molecular perspective of mammalian autophagosome biogenesis.* J Biol Chem, 2018. **293**(15): p. 5386-5395.
6. Karanasios, E. and N.T. Ktistakis, *Signalling in Autophagy*, in *Autophagy at the Cell, Tissue and Organismal Level*, S.i.C. Biology, Editor. 2016, Springer, Cham. p. 17-33.
7. Gatica, D., V. Lahiri, and D.J. Klionsky, *Cargo recognition and degradation by selective autophagy.* Nat Cell Biol, 2018. **20**(3): p. 233-242.
8. Allen, E.A. and E.H. Baehrecke, *Autophagy in animal development.* Cell Death Differ, 2020. **27**(3): p. 903-918.
9. Kuma, A., M. Komatsu, and N. Mizushima, *Autophagy-monitoring and autophagy-deficient mice.* Autophagy, 2017. **13**(10): p. 1619-1628.
10. Gomes, L.C. and I. Dikic, *Autophagy in antimicrobial immunity.* Mol Cell, 2014. **54**(2): p. 224-33.
11. Karanasios, E. and N.T. Ktistakis, *Physiological Role of Autophagy and Implications in Disease*, in *Autophagy at the Cell, Tissue and Organismal Level*, S. in and C. Biology, Editors. 2016, Springer, Cham. p. 51-80.
12. Hansen, M., D.C. Rubinsztein, and D.W. Walker, *Autophagy as a promoter of longevity: insights from model organisms.* Nat Rev Mol Cell Biol, 2018. **19**(9): p. 579-593.
13. Leidal, A.M., B. Levine, and J. Debnath, *Autophagy and the cell biology of age-related disease.* Nat Cell Biol, 2018. **20**(12): p. 1338-1348.
14. Fernández, Á., et al., *Disruption of the beclin 1-BCL2 autophagy regulatory complex promotes longevity in mice.* Nature, 2018. **558**(7708): p. 136-140.
15. Rubinsztein, D.C., P. Codogno, and B. Levine, *Autophagy modulation as a potential therapeutic target for diverse diseases.* Nat Rev Drug Discov, 2012. **11**(9): p. 709-30.
16. Menzies, F.M., A. Fleming, and D.C. Rubinsztein, *Compromised autophagy and neurodegenerative diseases.* Nat Rev Neurosci, 2015. **16**(6): p. 345-57.
17. Pickford, F., et al., *The autophagy-related protein beclin 1 shows reduced expression in early Alzheimer disease and regulates amyloid beta accumulation in mice.* J Clin Invest, 2008. **118**(6): p. 2190-9.
18. Lee, J.H., et al., *Lysosomal proteolysis and autophagy require presenilin 1 and are disrupted by Alzheimer-related PS1 mutations.* Cell, 2010. **141**(7): p. 1146-58.
19. Winslow, A.R., et al., *α-Synuclein impairs macroautophagy: implications for Parkinson's disease.* J Cell Biol, 2010. **190**(6): p. 1023-37.
20. Galluzzi, L., et al., *Autophagy in malignant transformation and cancer progression.* EMBO J, 2015. **34**(7): p. 856-80.
21. Mulcahy Levy, J.M. and A. Thorburn, *Autophagy in cancer: moving from understanding mechanism to improving therapy responses in patients.* Cell Death Differ, 2020. **27**(3): p. 843-857.

22. Takeshige, K., et al., *Autophagy in yeast demonstrated with proteinase-deficient mutants and conditions for its induction.* J Cell Biol, 1992. **119**(2): p. 301-11.
23. Klionsky, D.J., et al., *A unified nomenclature for yeast autophagy-related genes.* Dev Cell, 2003. **5**(4): p. 539-45.
24. Carroll, B., et al., *Control of TSC2-Rheb signaling axis by arginine regulates mTORC1 activity.* Elife, 2016. **5**.
25. Grasso, D., F.J. Renna, and M.I. Vaccaro, *Initial Steps in Mammalian Autophagosome Biogenesis.* Front Cell Dev Biol, 2018. **6**: p. 146.
26. Mercer, C.A., A. Kaliappan, and P.B. Dennis, *A novel, human Atg13 binding protein, Atg101, interacts with ULK1 and is essential for macroautophagy.* Autophagy, 2009. **5**(5): p. 649-62.
27. Ganley, I.G., et al., *ULK1.ATG13.FIP200 complex mediates mTOR signaling and is essential for autophagy.* J Biol Chem, 2009. **284**(18): p. 12297-305.
28. Hurley, J.H. and L.N. Young, *Mechanisms of Autophagy Initiation.* Annu Rev Biochem, 2017. **86**: p. 225-244.
29. Kim, J., et al., *Differential regulation of distinct Vps34 complexes by AMPK in nutrient stress and autophagy.* Cell, 2013. **152**(1-2): p. 290-303.
30. Matsunaga, K., et al., *Autophagy requires endoplasmic reticulum targeting of the PI3-kinase complex via Atg14L.* J Cell Biol, 2010. **190**(4): p. 511-21.
31. Axe, E.L., et al., *Autophagosome formation from membrane compartments enriched in phosphatidylinositol 3-phosphate and dynamically connected to the endoplasmic reticulum.* J Cell Biol, 2008. **182**(4): p. 685-701.
32. Bento, C.F., et al., *Mammalian Autophagy: How Does It Work?* Annu Rev Biochem, 2016. **85**: p. 685-713.
33. Dooley, H.C., et al., *WIPI2 links LC3 conjugation with PI3P, autophagosome formation, and pathogen clearance by recruiting Atg12-5-16L1.* Mol Cell, 2014. **55**(2): p. 238-52.
34. Gutierrez, M.G., et al., *Rab7 is required for the normal progression of the autophagic pathway in mammalian cells.* J Cell Sci, 2004. **117**(Pt 13): p. 2687-97.
35. Jiang, P., et al., *The HOPS complex mediates autophagosome-lysosome fusion through interaction with syntaxin 17.* Mol Biol Cell, 2014. **25**(8): p. 1327-37.
36. Wang, H., et al., *GABARAPs regulate PI4P-dependent autophagosome:lysosome fusion.* Proc Natl Acad Sci U S A, 2015. **112**(22): p. 7015-20.
37. Karanasios, E. and N.T. Ktistakis, *Autophagosome Formation*, in *Autophagy at the Cell, Tissue and Organismal Level*, S.i.C. Biology, Editor. 2016, Springer, Cham. p. 35-50.
38. Webber, J.L. and S.A. Tooze, *New insights into the function of Atg9.* FEBS Lett, 2010. **584**(7): p. 1319-26.
39. Saitoh, T., et al., *Atg9a controls dsDNA-driven dynamic translocation of STING and the innate immune response.* Proc Natl Acad Sci U S A, 2009. **106**(49): p. 20842-6.
40. Itakura, E., et al., *Structures containing Atg9A and the ULK1 complex independently target depolarized mitochondria at initial stages of Parkin-mediated mitophagy.* J Cell Sci, 2012. **125**(Pt 6): p. 1488-99.
41. Karanasios, E., et al., *Autophagy initiation by ULK complex assembly on ER tubulovesicular regions marked by ATG9 vesicles.* Nat Commun, 2016. **7**: p. 12420.
42. Orsi, A., et al., *Dynamic and transient interactions of Atg9 with autophagosomes, but not membrane integration, are required for autophagy.* Mol Biol Cell, 2012. **23**(10): p. 1860-73.
43. Young, A.R., et al., *Starvation and ULK1-dependent cycling of mammalian Atg9 between the TGN and endosomes.* J Cell Sci, 2006. **119**(Pt 18): p. 3888-900.
44. Guardia, C.M., et al., *Structure of Human ATG9A, the Only Transmembrane Protein of the Core Autophagy Machinery.* Cell Rep, 2020. **31**(13): p. 107837.

45. Tooze, S.A., *The role of membrane proteins in mammalian autophagy.* Semin Cell Dev Biol, 2010. **21**(7): p. 677-82.
46. Longatti, A., et al., *TBC1D14 regulates autophagosome formation via Rab11- and ULK1-positive recycling endosomes.* J Cell Biol, 2012. **197**(5): p. 659-75.
47. Koyama-Honda, I., et al., *Temporal analysis of recruitment of mammalian ATG proteins to the autophagosome formation site.* Autophagy, 2013. **9**(10): p. 1491-9.
48. Duke, E.M., et al., *Imaging endosomes and autophagosomes in whole mammalian cells using correlative cryo-fluorescence and cryo-soft X-ray microscopy (cryo-CLXM).* Ultramicroscopy, 2014. **143**: p. 77-87.
49. Chan, E.Y., et al., *Kinase-inactivated ULK proteins inhibit autophagy via their conserved C-terminal domains using an Atg13-independent mechanism.* Mol Cell Biol, 2009. **29**(1): p. 157-71.
50. He, S., et al., *PtdIns(3)P-bound UVRAG coordinates Golgi-ER retrograde and Atg9 transport by differential interactions with the ER tether and the beclin 1 complex.* Nat Cell Biol, 2013. **15**(10): p. 1206-1219.
51. Takahashi, Y., et al., *Bif-1 regulates Atg9 trafficking by mediating the fission of Golgi membranes during autophagy.* Autophagy, 2011. **7**(1): p. 61-73.
52. Takahashi, Y., et al., *The Bif-1-Dynamin 2 membrane fission machinery regulates Atg9-containing vesicle generation at the Rab11-positive reservoirs.* Oncotarget, 2016. **7**(15): p. 20855-68.
53. Søreng, K., et al., *SNX18 regulates ATG9A trafficking from recycling endosomes by recruiting Dynamin-2.* EMBO Rep, 2018. **19**(4).
54. Davies, A.K., et al., *AP-4 vesicles contribute to spatial control of autophagy via RUSC-dependent peripheral delivery of ATG9A.* Nat Commun, 2018. **9**(1): p. 3958.
55. Mattera, R., et al., *AP-4 mediates export of ATG9A from the.* Proc Natl Acad Sci U S A, 2017. **114**(50): p. E10697-E10706.
56. Mattera, R., et al., *The FTS-Hook-FHIP (FHF) complex interacts with AP-4 to mediate perinuclear distribution of AP-4 and its cargo ATG9A.* Mol Biol Cell, 2020. **31**(9): p. 963-979.
57. Zhou, C., et al., *Regulation of mATG9 trafficking by Src- and ULK1-mediated phosphorylation in basal and starvation-induced autophagy.* Cell Res, 2017. **27**(2): p. 184-201.
58. Lamb, C.A., et al., *TBC1D14 regulates autophagy via the TRAPP complex and ATG9 traffic.* EMBO J, 2016. **35**(3): p. 281-301.
59. Imai, K., et al., *Atg9A trafficking through the recycling endosomes is required for autophagosome formation.* J Cell Sci, 2016. **129**(20): p. 3781-3791.
60. Judith, D., et al., *ATG9A shapes the forming autophagosome through Arfaptin 2 and phosphatidylinositol 4-kinase IIIβ.* J Cell Biol, 2019. **218**(5): p. 1634-1652.
61. Alonso, A., et al., *The Extended Family of Protein Tyrosine Phosphatases.* Methods Mol Biol, 2016. **1447**: p. 1-23.
62. Gu, M., I. Warshawsky, and P.W. Majerus, *Cloning and expression of a cytosolic megakaryocyte protein-tyrosine-phosphatase with sequence homology to retinaldehyde-binding protein and yeast SEC14p.* Proc Natl Acad Sci U S A, 1992. **89**(7): p. 2980-4.
63. Dong, H.-b., et al., *Activity and tissue expression of tyrosine phosphatase PTP-MEG2.* Chem Res Chinese Universities, 2011. **27**(2): p. 287-90.
64. Crabb, J.W., et al., *Cloning of the cDNAs encoding the cellular retinaldehyde-binding protein from bovine and human retina and comparison of the protein structures.* J Biol Chem, 1988. **263**(35): p. 18688-92.

65. Crabb, J.W., et al., *Cellular retinaldehyde-binding protein ligand interactions. Gln-210 and Lys-221 are in the retinoid binding pocket.* J Biol Chem, 1998. **273**(33): p. 20712-20.
66. Wolf, G., *The intracellular vitamin A-binding proteins: an overview of their functions.* Nutr Rev, 1991. **49**(1): p. 1-12.
67. Aitken, J.F., et al., *The gene encoding the phosphatidylinositol transfer protein is essential for cell growth.* J Biol Chem, 1990. **265**(8): p. 4711-7.
68. Bankaitis, V.A., et al., *The Saccharomyces cerevisiae SEC14 gene encodes a cytosolic factor that is required for transport of secretory proteins from the yeast Golgi complex.* J Cell Biol, 1989. **108**(4): p. 1271-81.
69. Bankaitis, V.A., et al., *An essential role for a phospholipid transfer protein in yeast Golgi function.* Nature, 1990. **347**(6293): p. 561-2.
70. Qi, Y., et al., *Purification and characterization of protein tyrosine phosphatase PTP-MEG2.* J Cell Biochem, 2002. **86**(1): p. 79-89.
71. Kwok, V., E. Vachon, and G.P. Downey, *Use of fluorescent probes to detect lipid signaling intermediates in macrophages.* Methods Mol Biol, 2009. **531**: p. 301-28.
72. Kruger, J.M., et al., *Protein-tyrosine phosphatase MEG2 is expressed by human neutrophils. Localization to the phagosome and activation by polyphosphoinositides.* J Biol Chem, 2002. **277**(4): p. 2620-8.
73. Krugmann, S., et al., *Identification of ARAP3, a novel PI3K effector regulating both Arf and Rho GTPases, by selective capture on phosphoinositide affinity matrices.* Mol Cell, 2002. **9**(1): p. 95-108.
74. Huynh, H., et al., *Homotypic secretory vesicle fusion induced by the protein tyrosine phosphatase MEG2 depends on polyphosphoinositides in T cells.* J Immunol, 2003. **171**(12): p. 6661-71.
75. Zhao, R., et al., *Specific interaction of protein tyrosine phosphatase-MEG2 with phosphatidylserine.* J Biol Chem, 2003. **278**(25): p. 22609-14.
76. Sha, B., et al., *Crystal structure of the Saccharomyces cerevisiae phosphatidylinositol-transfer protein.* Nature, 1998. **391**(6666): p. 506-10.
77. Wang, X., et al., *Enlargement of secretory vesicles by protein tyrosine phosphatase PTP-MEG2 in rat basophilic leukemia mast cells and Jurkat T cells.* J Immunol, 2002. **168**(9): p. 4612-9.
78. Saito, K., et al., *Association of protein-tyrosine phosphatase MEG2 via its Sec14p homology domain with vesicle-trafficking proteins.* J Biol Chem, 2007. **282**(20): p. 15170-8.
79. Hay, J.C. and R.H. Scheller, *SNAREs and NSF in targeted membrane fusion.* Curr Opin Cell Biol, 1997. **9**(4): p. 505-12.
80. Söllner, T., et al., *A protein assembly-disassembly pathway in vitro that may correspond to sequential steps of synaptic vesicle docking, activation, and fusion.* Cell, 1993. **75**(3): p. 409-18.
81. Huynh, H., et al., *Control of vesicle fusion by a tyrosine phosphatase.* Nat Cell Biol, 2004. **6**(9): p. 831-9.
82. Mustelin, T., T. Vang, and N. Bottini, *Protein tyrosine phosphatases and the immune response.* Nat Rev Immunol, 2005. **5**(1): p. 43-57.
83. Wang, Y., et al., *Tyrosine phosphatase MEG2 modulates murine development and platelet and lymphocyte activation through secretory vesicle function.* J Exp Med, 2005. **202**(11): p. 1587-97.
84. Zhu, J., et al., *PTPN9 promotes cell proliferation and invasion in Eca109 cells and is negatively regulated by microRNA-126.* Oncol Lett, 2017. **14**(2): p. 1419-1426.

85. Du, W.W., et al., *MicroRNA miR-24 enhances tumor invasion and metastasis by targeting PTPN9 and PTPRF to promote EGF signaling.* J Cell Sci, 2013. **126**(Pt 6): p. 1440-53.
86. Hong, Y., et al., *miR-96 promotes cell proliferation, migration and invasion by targeting PTPN9 in breast cancer.* Sci Rep, 2016. **6**: p. 37421.
87. Su, F., et al., *Protein tyrosine phosphatase Meg2 dephosphorylates signal transducer and activator of transcription 3 and suppresses tumor growth in breast cancer.* Breast Cancer Res, 2012. **14**(2): p. R38.
88. Yuan, T., et al., *Protein-tyrosine phosphatase PTPN9 negatively regulates ErbB2 and epidermal growth factor receptor signaling in breast cancer cells.* J Biol Chem, 2010. **285**(20): p. 14861-70.
89. Hu, B., et al., *Downregulated Expression of PTPN9 Contributes to Human Hepatocellular Carcinoma Growth and Progression.* Pathol Oncol Res, 2016. **22**(3): p. 555-65.
90. Ying, D., Y. Ruan, and X. Zhou, *MEG2 inhibits the growth and metastasis of hepatocellular carcinoma by inhibiting AKT pathway.* Gene, 2019. **687**: p. 1-8.
91. Li, W.T., et al., *MiR-613 promotes cell proliferation and invasion in cervical cancer via targeting PTPN9.* Eur Rev Med Pharmacol Sci, 2018. **22**(13): p. 4107-4114.
92. Ma, X., et al., *MiR-96 enhances cellular proliferation and tumorigenicity of human cervical carcinoma cells through PTPN9.* Saudi J Biol Sci, 2018. **25**(5): p. 863-867.
93. Liu, Z., et al., *MEG2 is regulated by miR-181a-5p and functions as a tumour suppressor gene to suppress the proliferation and migration of gastric cancer cells.* Mol Cancer, 2017. **16**(1): p. 133.
94. Wang, D., et al., *PTPN9 induces cell apoptosis by mitigating the activation of Stat3 and acts as a tumor suppressor in colorectal cancer.* Cancer Manag Res, 2019. **11**: p. 1309-1319.
95. Cho, C.Y., et al., *Identification of the tyrosine phosphatase PTP-MEG2 as an antagonist of hepatic insulin signaling.* Cell Metab, 2006. **3**(5): p. 367-78.
96. Zhang, S., et al., *A highly selective and potent PTP-MEG2 inhibitor with therapeutic potential for type 2 diabetes.* J Am Chem Soc, 2012. **134**(43): p. 18116-24.
97. Bu, Y., et al., *Protein tyrosine phosphatase PTPN9 regulates erythroid cell development through STAT3 dephosphorylation in zebrafish.* J Cell Sci, 2014. **127**(Pt 12): p. 2761-70.
98. Huang, X., et al., *Regulated expression of microRNAs-126/126* inhibits erythropoiesis from human embryonic stem cells.* Blood, 2011. **117**(7): p. 2157-65.
99. Xu, M.J., et al., *PTP-MEG2 is activated in polycythemia vera erythroid progenitor cells and is required for growth and expansion of erythroid cells.* Blood, 2003. **102**(13): p. 4354-60.
100. Hao, Q., et al., *Tyrosine phosphatase PTP-MEG2 negatively regulates vascular endothelial growth factor receptor signaling and function in endothelial cells.* Am J Physiol Cell Physiol, 2012. **303**(5): p. C548-53.
101. Qu, M., et al., *MicroRNA-126 Regulates Angiogenesis and Neurogenesis in a Mouse Model of Focal Cerebral Ischemia.* Mol Ther Nucleic Acids, 2019. **16**: p. 15-25.
102. Reinhard, J., et al., *Protein tyrosine phosphatases expression during development of mouse superior colliculus.* Exp Brain Res, 2009. **199**(3-4): p. 279-97.
103. Zhang, D., et al., *The Protein Tyrosine Phosphatase MEG2 Regulates the Transport and Signal Transduction of Tropomyosin Receptor Kinase A.* J Biol Chem, 2016. **291**(46): p. 23895-23905.
104. Ran, F.A., et al., *Genome engineering using the CRISPR-Cas9 system.* Nat Protoc, 2013. **8**(11): p. 2281-2308.

105. Wei, Y., et al., *EGFR-mediated Beclin 1 phosphorylation in autophagy suppression, tumor progression, and tumor chemoresistance.* Cell, 2013. **154**(6): p. 1269-84.
106. Hirsch, D.S., et al., *Insulin activation of vacuolar protein sorting 34 mediates localized phosphatidylinositol 3-phosphate production at lamellipodia and activation of mTOR/S6K1.* Cell Signal, 2014. **26**(6): p. 1258-68.
107. Ratz, M., et al., *CRISPR/Cas9-mediated endogenous protein tagging for RESOLFT super-resolution microscopy of living human cells.* Sci Rep, 2015. **5**: p. 9592.
108. Roux, K.J., et al., *A promiscuous biotin ligase fusion protein identifies proximal and interacting proteins in mammalian cells.* J Cell Biol, 2012. **196**(6): p. 801-10.
109. Roux, K.J., D.I. Kim, and B. Burke, *BioID: a screen for protein-protein interactions.* Curr Protoc Protein Sci, 2013. **74**: p. 19.23.1-19.23.14.